

## INFALLING FAINT [O II] EMITTERS IN ABELL 851. II. ENVIRONMENT, KINEMATICS, & STAR FORMATION HISTORY

TARO SATO<sup>1</sup> AND CRYSTAL L. MARTIN<sup>2,3,4</sup>

Department of Physics, University of California, Santa Barbara, CA 93106-9530

*To appear in Astrophysical Journal*

### ABSTRACT

We report on the local environment, radial velocity, and star formation history of [O II]-selected emission-line objects in the  $z \approx 0.4$  galaxy cluster Abell 851, using optical spectra obtained with Keck I/LRIS and Keck II/DEIMOS. A large fraction ( $\approx 55\%$ ) of cluster [O II] emitters show strong Balmer absorption lines ( $\gtrsim 4 \text{ \AA}$  in equivalent width at H $\delta$ ). These e(a)-type spectra have been attributed to dusty starburst galaxies by Poggianti & Wu (2000), an interpretation supported by our Balmer-decrement–derived reddening measurements, which show a high frequency of very reddened [ $E(B-V) \gtrsim 0.5$ ] [O II] emitters. Our spectral modeling requires starburst ages  $\lesssim 1$  Gyr, which is shorter than the cluster crossing timescale. We argue that this starburst phase occurs during cluster infall based on the radial velocity distribution of the cluster [O II] emitters, which present a deficit of systems near the cluster systemic velocity compared to a virialized population (or a backslash population). The spatial segregation of some redshifted and blueshifted groups strongly indicates that the accretion was recent. Throughout the cluster, the fraction in [O II]-emitting galaxies is a strong function of the local galaxy density, being suppressed in dense environments. Our analysis supports previous suggestions that dusty starburst galaxies arise at the expense of continuously star-forming gas-rich spiral galaxies [i.e., the e(c)-type; Dressler et al. (1999)]. In addition, we describe a fainter [O II]-emitting population, comprised largely of dwarf galaxies (Martin et al. 2000) and find an even stronger suppression of [O II] emission in high density environments among this subsample, indicative of more effective destruction by harassment and/or gas-stripping. Comparison to previous morphological studies, limited to the central region of Abell 851, suggests that galaxy-galaxy interactions may trigger the starbursts. The high e(a) galaxy fraction in Abell 851 compared to that in the field, however, suggests that some cluster-specific mechanism, likely related to the dynamical assembly of the cluster, also contributes to the high number of starbursts.

*Subject headings:* galaxy cluster: general — galaxies: clusters: individual (Abell 851; CL0939+4713) — galaxies: dwarf — galaxies: evolution — galaxies: starburst — cosmology: observations

### 1. INTRODUCTION

Local environment has a strong effect on the star-forming activity and morphology of galaxies—the observation first recognized in the cores of rich clusters (Dressler 1980; Butcher & Oemler 1984). There is mounting evidence in support for the Butcher-Oemler effect (Butcher & Oemler 1984) as a cosmic process, not specific to galaxy clusters, in which the field-to-cluster transformation of galaxies occurs upon the accretion of field galaxies to cluster central regions (Dressler et al. 1994; Couch et al. 1994; Abraham et al. 1996; Ellingson et al. 2001; Tran et al. 2004). In fact, recent studies of cluster galaxies have shown that mechanisms responsible for their transformation must be in effect well beyond cluster virial radii, well before the galaxies at infall reach the central regions of clusters (e.g., Balogh et al. 1997; Treu et al. 2003; Rines et al. 2005; Moran et al. 2005; Pimblet et al. 2006). Since cluster environment samples a wide range in local galaxy density and relative velocity of cluster members, a dominant physical process driving galaxy evolution may vary over an infall period. Thus most recent efforts in cluster galaxy surveys have focused on studying galaxies in infall regions where the preprocessing of cluster galaxies is already in effect.

Although the studies spanning a few decades have estab-

lished such empirical relations as the morphology-density relation (Dressler 1980) and the Butcher-Oemler effect (Butcher & Oemler 1984) for giant luminous cluster galaxies, the underlying physical processes that are responsible for the transformation of their properties and therefore the aforementioned empirical relations have yet to be well constrained to date. The sign of the differential evolution between dwarf and giant galaxies is even more obscure, since few wide-field surveys have sampled faint galaxies at high redshift. Dwarf and large spiral galaxies are expected to respond differently to cluster tidal fields due to their different mass concentrations (Moore et al. 1999). In predicting a steep halo mass function, the currently standard hierarchical galaxy formation models (e.g., Kauffmann et al. 1993; Cole et al. 1994) produce more dwarf galaxies than actually observed (e.g., Klypin et al. 1999; Somerville 2002). Galaxy clusters host dense environments that are hostile to fragile dwarf galaxies; therefore the apparent faint-end steepening of cluster galaxy luminosity function presents a challenge to dwarf formation models (see, e.g., Popesso et al. 2005, and references therein).

Redshift surveys of local universe and  $N$ -body simulations show that large-scale filaments are a natural product of gravitationally driven structure formation (e.g., Bond et al. 1996; Rines et al. 2001; Pimblet et al. 2004). Galaxy clusters are expected to form at the intersections of filamentary structures, yet there has been few studies on the direct detection of filaments extending out from isolated clusters at high redshifts (e.g., Ebeling et al. 2004). A rich, moderately distant ( $z \approx 0.4069$ ) galaxy cluster Abell 851 [CL0939+4713;  $9^{\text{h}}42^{\text{m}}56^{\text{s}}.2$ ,

<sup>1</sup> taro@physics.ucsb.edu

<sup>2</sup> cmartin@physics.ucsb.edu

<sup>3</sup> Packard Fellow

<sup>4</sup> Alfred P. Sloan Foundation Fellow

46°59'12"0 (J2000)] offers evidence of filaments, observed via the photometric redshift technique (Kodama et al. 2001, hereafter K01). Since few clusters at this epoch have been studied well beyond their virial radii, it remains unclear whether the observed structures are actually filaments of cosmological origin or are related to on-going merger event (De Filippis et al. 2003). In either case, Abell 851 presents a unique opportunity to study cluster galaxy evolution in a dynamically active environment on the large scales.

Before the identification of the filaments, Abell 851 had already drawn attention due to the extreme richness (e.g., Gunn et al. 1986) and high abundance of blue, star-forming galaxies; the cluster contains a larger fraction in young emission-line galaxies compared to clusters at similar redshift (Lotz et al. 2003). A spectroscopic survey of  $r \lesssim 22.5$  galaxies revealed a high fraction in post-starburst galaxies, whose spectra are dominated by Balmer absorption lines of intermediate-age stars (Dressler et al. 1999, hereafter D99). The timescales associated with such galaxies implied the suppression of star-forming activity within the past  $\sim 1.5$  Gyr. Since the cluster crossing time for infalling galaxies is at least a few Gyr (Treu et al. 2003) and definitely longer than the post-starburst timescales, the high abundance of post-starburst galaxies suggested the significance of cluster-induced starburst in the transformation of cluster galaxies. Although the scarcity of star-forming activity in very dense environments within the central regions of clusters has been universally observed and confirmed, there has been a debate as to the existence of enhanced starburst phase *before* the suppression of star-forming activity of infalling cluster galaxies kicks in (Dressler et al. 1999; Balogh et al. 1999; Tran et al. 2003, 2004). In post-starburst galaxies, we see remnants of starbursts, but detecting the signs of starbursts is generally complicated by the need for constraining the star formation history (SFH) of galaxies—the process requiring more than a simple diagnostics of star-forming activity.

Martin et al. (2000, hereafter MLF00) carried out narrowband and broadband photometry of Abell 851 using Mayall 4-meter telescope at the Kitt Peak National Observatory, to detect faint emission-line galaxies using their redshifted [O II] $\lambda$ 3727 emission line. The narrowband search yielded 371 emission-line cluster member candidates. The completeness limit of the MLF00 survey was  $g \simeq 24.5$ , about ten times deeper than the D99 spectroscopic survey. The locus in the  $(g-i)$ - $i$  color-magnitude diagram and their small isophotal area suggested their dwarf identity for a significant fraction of the [O II] emission candidates. In a spectroscopic follow-up program of the MLF00 survey, we have obtained an extensive set of spectra of the [O II]-emitting candidates using the Keck I Low Resolution Imaging Spectrometer (LRIS; Oke et al. 1995) and Keck II Deep Imaging Multi-Object Spectrograph (DEIMOS; Faber et al. 2003).

As the second in a series of papers drawing on the Keck spectroscopic sample of the [O II] emitters, we present the analysis of environment, kinematics properties, and SFH of infalling faint star-forming galaxies in a highly dynamically active galaxy cluster at  $z \simeq 0.4$ . The observations, data, and the spectroscopic confirmation of MLF00 [O II] emitters have been reported in Sato & Martin (2006, hereafter Paper I), to which readers are referred for the detailed information on the basic characteristics of our spectroscopic sample. This paper starts with the sections entirely dedicated to the effect of local environment (§ 2) and the kinematic properties (§ 3) of cluster [O II] emitters. In § 4 we present the cluster [O II] emitters in

terms of their spectral types derived from the [O II] emission and H $\delta$  absorption equivalent widths, which will be analyzed in view of photoionization and stellar population synthesis models in § 5. We then discuss (§ 6) and summarize (§ 7) our results.

Throughout this paper, we use the standard  $\Lambda$ CDM cosmology,  $(\Omega_m, \Omega_\Lambda) = (0.3, 0.7)$ , with  $H_0 = 70 \text{ km s}^{-1} \text{ Mpc}^{-1}$ . At the distance of Abell 851 ( $z = 0.4069$ ),  $1''$  on the sky corresponds to a projected physical distance of 5.43 kpc, and the lookback time to the galaxy cluster is 4.3 Gyr.

## 2. EFFECTS OF LOCAL ENVIRONMENT

The star-forming property of a galaxy has been shown to depend strongly on its local environment, often quantified by the projected number density of galaxies near the apparent position of the galaxy in the sky. For Abell 851 in particular, K01 have reported a so-called threshold effect—galaxy  $V-I$  colors abruptly become redder above a threshold density,  $\sim 50 \text{ galaxies Mpc}^{-2}$  (in the cosmology assumed in this paper), which roughly corresponds to the typical local galaxy density within the substructures in surrounding filaments.<sup>5</sup> Robust determinations of cluster memberships are essential for quantifying local environment of cluster galaxies. We obtained the photometry and photometric redshifts of the objects studied in K01, kindly provided by T. Kodama. The K01 survey limiting magnitude was roughly comparable to our survey:  $I(\text{AB}) \simeq 23.4$  (K01) and  $i \simeq 23$  (MLF00); this is quite deep, as K01 estimates  $M_V^*$  to be about  $I = 19.4$  in this cluster.

### 2.1. Local Projected Density of Galaxies

The local environment of a galaxy is quantified by a projected surface galaxy number density,  $\Sigma$ , using ten nearest cluster members defined by K01 via the photometric redshift method. The value is computed for each galaxy in our survey as follows: (1) Using the RA and DEC of a galaxy, we find ten K01 confirmed cluster members nearest to that position; (2) compute the distance between the farthest and closest members to that reference coordinates in the ten objects just found; and (3) take that as the radius of a circular projected area by which the number of galaxies within the area (i.e., always 10) is divided. The only difference from the conventional method is that our ten-nearest neighbor density may or may not include the galaxy for which the value is computed. This is because explicit spatial cross-correlation was not made between the MLF00 and K01 objects, but the deviation does not significantly alter the conclusions drawn from our study. K01 estimated the field contamination to the projected density of cluster galaxies in their survey to be  $2.29 \pm 0.06 \text{ arcmin}^{-2}$ . We statistically subtracted this from our computation of local galaxy density described above. In the nearest-neighbor approach, the effect of Poissonian uncertainty in the expected number of field galaxies becomes dominant for smaller  $\Sigma$ , since the area enclosing ten cluster members contains many more non-member objects. A  $1\sigma$  Poisson uncertainty in the field contamination becomes comparable to the local density estimate for a cluster member at  $\log \Sigma \simeq 0.3$ . The systematic removal of field contamination yields unphysical value of  $\Sigma < 0 \text{ Mpc}^{-2}$  for some galaxies. Where required, we generally assigned  $\log \Sigma = -2$  as the upper limit for such galaxies.

<sup>5</sup> We caution that local galaxy densities computed in such a method used in our study may not be directly compared to those in other surveys; a projected density estimate derived from a nearest-neighbor approach is highly sensitive to the specific ways in which foreground and background galaxies are removed from a cluster sample.

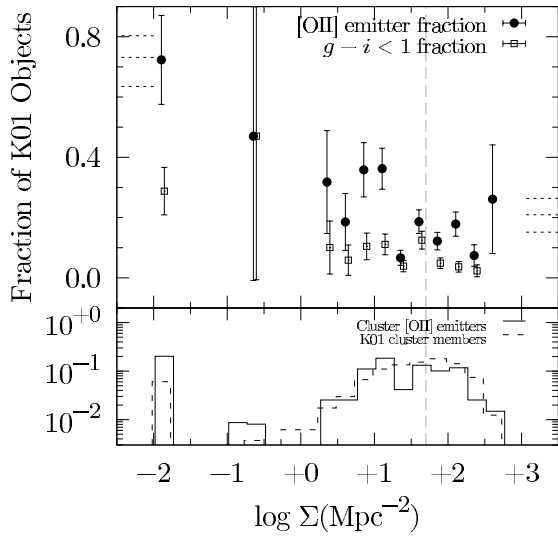


FIG. 1.— (Top) The [O II] emitter fractions (filled circles) as a function of local galaxy density  $\Sigma$ . The fractions of [O II] emitters in  $g-i < 1$  galaxies (open squares) are also shown. The fractions are computed from the number of spectroscopically-confirmed [O II] emitters (multiplied by appropriate correction factors given in Paper I to account for the selection bias) normalized to the number of K01 cluster members at each density bin. Dotted horizontal lines indicate the best estimates and  $1\sigma$  uncertainties for the fractions of galaxies with  $W_0([\text{O II}]) < -10 \text{ \AA}$  in cluster and field samples at  $z \approx 0.4$  computed by Nakata et al. (2005). (Bottom) Fractional abundance as a function of local galaxy density for the spectroscopically-confirmed cluster [O II] emitters corrected for the target selection bias ( $N \approx 175$ ; solid histogram) and the K01 cluster members ( $N = 808$ ; dashed histogram). The fractional abundance is normalized to the total number of objects ( $N$ ) within each sample to facilitate the comparison of density distributions. The vertical gray dashed line indicates the threshold density,  $\log \Sigma \approx 1.7$ , over which  $V-I$  colors of galaxies become redder as reported by K01.

## 2.2. [O II] Emitter Fraction

We start with a brief summary of the basic properties of the cluster [O II]-emitting sample presented in Paper I. Our cluster [O II] emitters for this spectroscopic follow-up were drawn from 371 narrowband-selected objects with their candidate [O II] emission detected at  $S/N > 3$  level in MLF00. The narrowband survey was roughly complete to the observed equivalent width of  $\lesssim -11 \text{ \AA}$  at  $m_{5129}(\text{AB}) \approx 24.6$ . The preference was given to the objects with bluer  $g-i$  colors (i.e.,  $g-i < 1$ ), so the sample is more complete for blue objects. Among the 212 objects selected for spectroscopic follow-up, 111 actually showed [O II] emission and had redshifts within the range  $z = 0.395-0.420$ , constituting our cluster [O II]-emitting sample. This final sample spans a wide range in luminosity,  $18.5 \lesssim i \lesssim 25.5$ , where  $i \approx 23$  corresponds to the completeness limit of the MLF00 narrowband survey.

Fig. 1 shows the distributions of cluster [O II] emitters and the K01 cluster members within the survey area of MLF00. Note that the histogram for the spectroscopically-confirmed cluster [O II] emitters are corrected for the target selection bias by the  $g-i$  color, i.e., we multiply the number actually observed by the correction factor for each  $g-i$  color subsample; see Paper I for the details. A Kolmogorov-Smirnov (K-S) test of the distributions of local galaxy density for the spectroscopically-confirmed cluster [O II] emitters and more general, photo- $z$ -selected cluster population from K01 yields a very small probability ( $\ll 1\%$ ) that they share a common parent distribution. This indicates the [O II]-emitting population resides in different environments than the general clus-

<sup>6</sup> An equivalent width of an emission line is designated a negative sign; see Paper I for the sign and other notational conventions used in this paper.

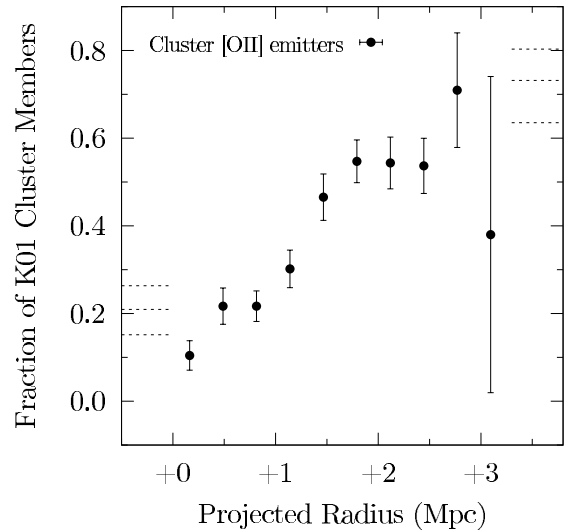


FIG. 2.— The [O II] emitter fraction of K01 photo- $z$  cluster members as a function of projected radius from the cluster center. The center of the cluster was taken to be at  $9^{\text{h}}43^{\text{m}}03^{\text{s}}.3$ ,  $46^{\circ}59'26''.5$  (J2000), corresponding to the brightest point in X-ray surface brightness from De Filippis et al. (2003). Dotted horizontal lines indicate the best estimates and  $1\sigma$  uncertainties for the fractions of galaxies with  $W_0([\text{O II}]) < -10 \text{ \AA}$  in cluster and field samples at  $z \approx 0.4$  computed by Nakata et al. (2005). At each radial bin, the fraction is corrected for MLF00 emission-line candidates not spectroscopically observed, in addition to the usual target selection correction by  $g-i$  colors (Paper I).

ter galaxy population. A relatively higher fraction of cluster [O II] emitters is found at low densities. The emission-line galaxy fraction has been shown observationally to depend strongly on local environments, where a smaller fraction is observed in dense environments (e.g., Balogh et al. 2004b). Furthermore, such an emission-line galaxy fraction appears to evolve with redshift (Kodama et al. 2004; Nakata et al. 2005).

At the lowest density bin, the fraction in [O II] emitters matches well the field [O II] emitter fraction at  $z \sim 0.4$  of  $\sim 70\%$  estimated by Nakata et al. (2005) from their sample drawn from the Canadian Network for Observational Cosmology 1 (CNOC1) cluster survey; the [O II] equivalent width cut for their [O II]-emitting population is similar to ours [ $W_0([\text{O II}]) < -10 \text{ \AA}$ ]. As discussed in Paper I, MLF00 could have detected only  $\sim 75\%$  of virialized cluster [O II] emitters with their narrowband filter, assuming a Gaussian velocity distribution for virialized cluster members. In Fig. 1, we did not statistically correct for this population which could have been missed by the MLF00 narrowband survey. Although we do not expect the MLF00 survey area ( $4.4 \text{ Mpc} \times 4.4 \text{ Mpc}$ ) to be large enough for sampling a true field population and applied a crude correction for target selection bias, the sampling at low-density region appears to provide us with a reasonable [O II]-emitting sample in field-like environments, since their observed fraction is consistent with the independent measurement of field [O II] emitter fraction.

The [O II] emitter fraction in the densest environment in our sample,  $\sim 20\%$ , is also roughly consistent with the observed [O II] emitter fraction in  $z = 0.4$  clusters (Nakata et al. 2005). In relation to the K01 threshold density at which the  $V-I$  colors of cluster galaxies have been shown to become red quite abruptly, the presence of [O II] emitters appears already suppressed at slightly lower densities, and their fraction remains roughly constant at the lowest level toward denser environments. Fig. 2 shows the [O II] emitter fraction as a function of projected radius from the cluster center. The radial trend

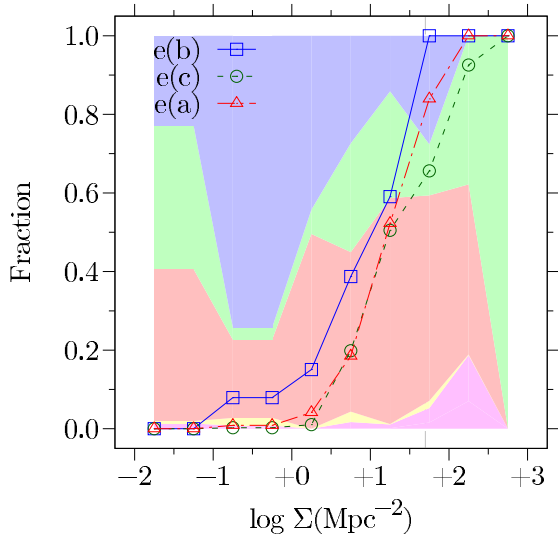


FIG. 3.— Cumulative local density distributions of the cluster [O II] emitters with various D99 spectral types: e(b) (open squares), e(c) (open circles), and e(a) (open triangles). The distribution is normalized to zero at the field value (i.e., at the lowest density bin) for each spectral type. The samples are binned with constant  $\log \Sigma = 0.5$  intervals, where the symbols in the plot indicates their central values. The spectral types are assigned using the best estimates as well as the uncertainties in [O II] and H $\delta$  measurements (see § 4.2 for detail). The fractions are corrected for the target selection bias by appropriate correction factors (Paper I). In the electronic edition, the relative abundances of the [O II] cluster emitters in different D99 spectral types are also indicated by the filled curves: from the top, they are e(b) (blue), e(c) (green), e(a) (red), k (yellow), and k+a/a+k (magenta). The colors are half-toned for better contrast. [See the electronic edition of the paper for a color version of this figure.]

is expected in view of Fig. 1, since the local galaxy density is generally anti-correlated with the cluster radius.

The distribution of  $g-i < 1$  galaxies among the [O II] emitters shows a modest peak near the K01 threshold density. It is hard to see whether this peaking is directly related to the threshold effect, but it could indicate the presence of starbursts as galaxies enter local environments typical of cluster substructures. In Fig. 3, we see the cumulative local density distributions of the cluster [O II] emitters with various D99 spectral types. According to  $\chi^2$  tests, the cumulative distributions among e(b), e(c), and e(a) types are different at very high confidence levels ( $\gg 99\%$ ). The details of the D99 classification scheme will be discussed in § 4.2, but for the current discussion, we note that e(b), e(a), and k+a/a+k galaxies are all associated with starbursts, whereas e(c) and k galaxies are not. Fig. 3 may provide additional evidence for a higher incidence of starbursts in the local environments near the K01 threshold of  $\log \Sigma \simeq 1.7$ . We also note a striking drop in the [O II] emitter fraction at  $\log \Sigma \approx 1.3$ , not too far from the K01 threshold density. Although a very strong suppression of star-forming activity near the K01 threshold could be real, the [O II] emitter and  $g-i < 1$  galaxy fraction are already well below the field values at  $\log \Sigma \approx 0.5$ ; therefore, some mechanism of quenching star formation could be in effect below the K01 threshold density as well.

### 2.3. [O II] & H $\alpha$ Equivalent Width Distribution

Although the star-forming galaxy fraction strongly depends on local environments, in previous studies the amount or strength of star-forming activity within each galaxy, probed via such emission-line diagnostics as H $\alpha$  equivalent width, does not appear to depend strongly on local environments (Balogh et al. 2004a,b; Kodama et al. 2004; Rines et al. 2005).

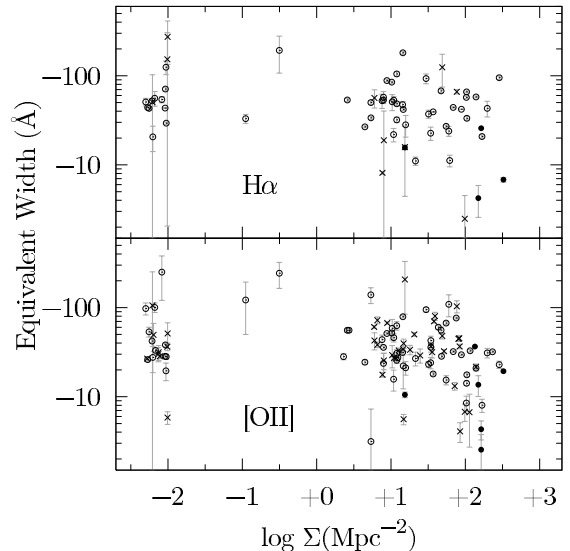


FIG. 4.— Rest-frame [O II] $\lambda 3727$  (bottom) and H $\alpha$  (top) equivalent widths of cluster [O II] emitters as a function of their local galaxy density. Open and filled circles are H II region-like galaxies and AGN-like objects, respectively; crosses are the objects whose classification by the line ratio diagnostics could not be carried out. See Paper I for the method used for these identifications. For the data points with  $\log \Sigma = -2$ , small negative random numbers are added to their densities to avoid excessive overlapping.

In Fig. 4 we see how our cluster [O II]-emitting sample compares. For the wide dynamic range in local galaxy densities, almost five decades in  $\Sigma$ , the strength of [O II] and H $\alpha$  equivalent widths shows only a mild decrease at high densities. The lack of dependence on local galaxy densities becomes more remarkable in view of Fig. 5, where luminous [O II] emitters—many of which are found to be AGN-like (Paper I)—have weaker [O II] and H $\alpha$  equivalent widths. The high abundance of luminous AGN-like [O II] emitters at high densities significantly accounts for the apparent trend.

Relative independence of the strength of emission equivalent widths of star-forming galaxies on their local galaxy density, combined with the strong trend of decreasing [O II] emitter fraction with local galaxy density, has given rise to an interpretation that the mechanisms that halt star-forming activity in these galaxies either work on very short timescales and/or are sufficiently rare that we are not seeing an abundance of galaxies in transition from actively star-forming to passively-evolving states. Starbursts followed by quenching of star-formation offers an attractive solution in this regard. A fraction of total galaxies in the starburst or post-starburst phase could offer an insight, yet the existing surveys have shown considerable disagreements as to the frequency of starburst and/or post-starburst galaxies (Dressler et al. 1999; Balogh et al. 1999; Tran et al. 2003, 2004). Even with a robust estimate of post-starburst fraction, the role of post-starburst phase in galaxy evolution is still obscure. Nonetheless our cluster [O II]-emitting sample offers no contradicting evidence to either of the above interpretations.

### 2.4. Luminosity Distribution

In Fig. 5 we see the distribution of cluster [O II] emitters in terms of their luminosity and local environment. Interestingly, it shows that among our cluster [O II] emitters AGN-like galaxies are luminous and mostly reside in dense environments. However, we must caution that within the intermediate luminosity range there are a number of galaxies for which we could not carry out line-ratio diagnostics for AGN

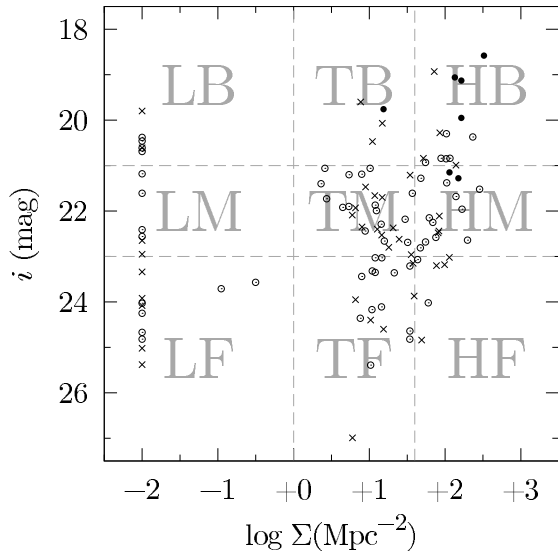


FIG. 5.— The  $i$  magnitudes of cluster [O II] emitters as a function of their local galaxy density. Symbols are as in Fig. 4. Grids of the  $i$ - $\Sigma$  plane defines the subsamples of cluster [O II] emitters to be coadded (§ 5.2). The magnitude cuts are made at  $i = 21$  and 23, and the density cuts are at  $\log \Sigma = 0$  and 1.6. Objects are divided into nine subsamples by their  $\log \Sigma$ : low-density (L), transitional (T), and high-density (H) environments; and by their luminosity: bright (B), medium (M), and faint (F) in term of  $i$  magnitude.

activity (Paper I), indicated by crosses in the figure. Also, none of the cluster [O II] emitters are spatially coincident with the *XMM-Newton* X-ray point sources detected at the level of  $L_X(\text{bol}) \gtrsim 1.6 \times 10^{43} \text{ erg s}^{-1}$  by De Filippis et al. (2003). The X-ray observation does not exclude the possibility of these galaxies hosting nuclear activities, however. In Fig. 6 we see the AGN-like galaxies in our sample have  $g-i > 1$ , putting them in the reddest end of the distribution of SDSS red AGNs, which generally appear X-ray weak as well (Brandt et al. 2004). If the observed trend of AGN-like galaxy distribution is real, it would point to the significant role of optically-luminous AGN-like galaxies in dense environments, whose [O II] emission equivalent widths are generally smaller than those of more general star-forming galaxy population (Paper I). As mentioned in Paper I, if AGN feedback acts to suppress star formation in luminous (or massive) galaxies, that offers a possible explanation for the *downsizing effect*, which refers to observational evidence for the redshift evolution of characteristic galaxy luminosity above which star-forming activities are suppressed (Cowie et al. 1996).

It is also notable that we see relatively few low-luminosity galaxies in dense environments, in the region marked as HF in Fig. 5. Although the range  $i > 23$  is below the completeness limit of narrowband survey, the depletion of faint galaxies at high densities is remarkable because of the abundance of galaxies with similar luminosities in lower-density environments. The relative depletion of faint galaxies in high-density environments here simply means the lack of star-forming population, and can result from suppressed star-forming activity in faint galaxies, which simply fade out of our survey limit, or their true absence, possibly due to the destruction of low surface brightness dwarf galaxies within a strong cluster gravitational potential or by a series of impulsive gravitational encounters with other galaxies—so-called galaxy harassment (Moore et al. 1999). The  $i$ -band magnitude of our [O II] emitters samples their rest-frame  $V$ -band light, which itself depends on the amount of on-going star-forming activity. Since our survey is insensitive to the non-star-forming population,

we cannot rigorously exclude or favor either of the two possibilities.

In Paper I we showed the strength of [O II] equivalent width shows only a mild decreasing trend with luminosity. In dense environments, the absence of strong [O II] emitters is partially a consequence of the lack of faint [O II] emitters and the presence of optically-luminous AGN-like galaxies with moderate to weak [O II] equivalent widths. This environmental trend of [O II]-emitting population makes stronger the claim that the amount of star-forming activity in star-forming galaxies does not vary much in different local environments, while the star-forming galaxy fraction is a strong function of local environment. The luminosity segregation of galaxy populations in dense environments further suggests the importance of differential evolution of galaxies based on their intrinsic properties.

### 3. KINEMATICS OF THE CLUSTER [O II] EMITTERS

Studying the connections between galaxies and their host environments in galaxy clusters helps to understand the transformation of galaxies in cosmological context. Cluster galaxy populations in relation to projected cluster-centric radii and galaxy local number densities are relatively easier to quantify and therefore have been well studied (e.g., Oemler 1974; Melnick & Sargent 1977; Treu et al. 2003). The relations between cluster galaxy populations and their kinematics, however, are nontrivial since cluster galaxies are not necessarily in dynamical equilibrium on the scale of an entire cluster. Whereas projected cluster-centric radii set lower limits on the true distances of cluster members from the cluster dynamical center, observed line-of-sight velocities say little about their relative locations to the cluster, not to mention obtaining a number of redshifts requires observationally expensive spectroscopic surveys. As the connections between the morphology-radius and morphology-density relations and the hierarchical picture of structure formation become clearer, it is of great interest to better constrain the relations between the dynamical states of clusters and their effect on constituent cluster galaxies.

In this section, we analyze the kinematic states of cluster [O II] emitters. This population is compared to the spectroscopically-confirmed early-type galaxy population from the D99 survey to shed more light on the connections between the dynamical states and the star-forming property of cluster [O II] emitters. Although the size of D99 spectroscopic sample is small,  $N = 31$  for k-type galaxies (see § 4.1 for definition of spectral types), comparing the [O II] emitters to the galaxies composed of much older stellar population observed in the same cluster illuminates the kinematic segregation of galaxies with different ages often reported in literature. These two classes of galaxies are clearly separated in the  $(g-i)$ - $i$  color-magnitude diagram (Fig. 6), and most D99 k-type galaxies belong to a well-defined cluster red sequence.

#### 3.1. Velocity Distribution

For each cluster [O II] emitter we computed its cluster-centric line-of-sight velocity (or simply radial velocity) in the rest-frame of cluster:

$$\Delta v_{\text{los}} \equiv c \frac{z - z_{\text{cl}}}{1 + z_{\text{cl}}},$$

where  $z$  is the observed redshift of the galaxy and  $z_{\text{cl}} = 0.4069$  for Abell 851. Fig. 7 shows the velocity distribution of cluster [O II] emitters and D99 cluster member galaxies. It is quite obvious that the velocity distribution of our cluster [O II] emitters is not well described by a Gaussian. A

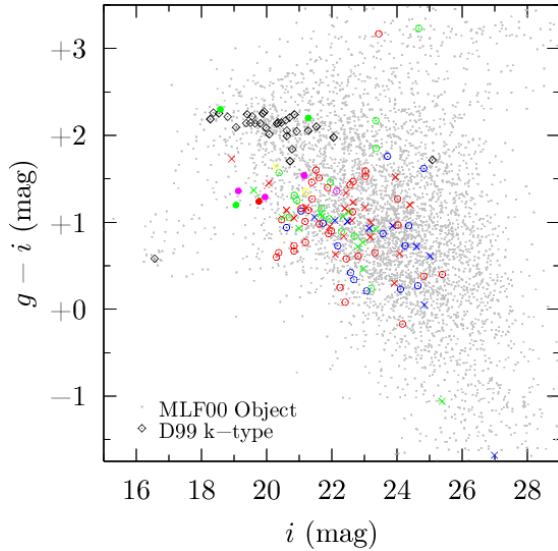


FIG. 6.— The  $(g-i)$ - $i$  color-magnitude diagram of all MLF00 objects detected in their broadband images (gray dots), D99 k-type galaxies (open diamonds), and cluster [O II] emitters (symbols as in Fig. 4). The  $g-i$  colors and  $i$  magnitudes of D99 objects are determined by those of spatially cross-correlated objects in the MLF00 catalog, which includes the  $g-i$  colors of all the objects detected in their broadband images. In the color version, the D99 spectral types for the [O II] emitters (§ 4) from the best estimates of the [O II] and H $\delta$  equivalent widths are indicated by blue [e(b)], green [e(c)], red [e(a)], yellow (k), and magenta (k+a/a+k). [See the electronic edition of the paper for a color version of this figure.]

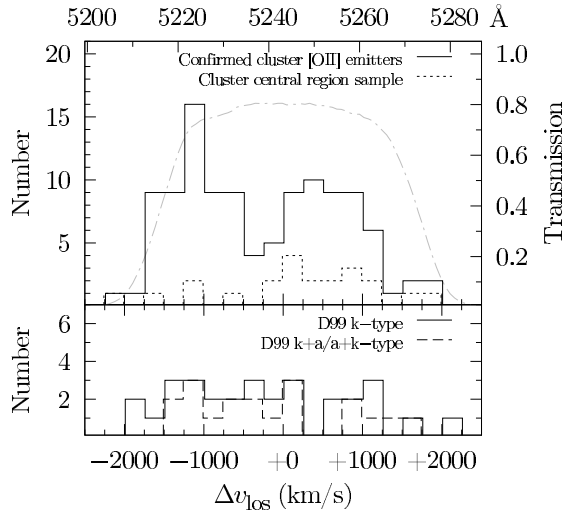


FIG. 7.— (Top) Cluster rest-frame line-of-sight velocity distribution of cluster [O II] emitters. The solid histogram corresponds to the spectroscopically-confirmed cluster members with [O II] emission, and the short-dashed histogram is that of cluster [O II] emitters within the common survey area with D99. Top axis corresponds to the central wavelength of redshifted [O II] emission line. The MLF00 on-band filter transmission curve is shown in a gray dash-dotted line with the transmission efficiency indicated on the right axis. (Bottom) The velocity distribution of the confirmed Abell 851 members with a k- (solid histogram) and k+a/a+k-type spectrum (long-dashed histogram) from D99.

virialized population is expected to have a Gaussian velocity distribution around the cluster systemic velocity. A K-S test on the distribution of [O II] emitters rejects a Gaussian at a very high confidence level ( $> 99\%$ ). A peculiar feature of the velocity distribution of cluster [O II] emitters (e.g.,  $-500 \text{ km s}^{-1} < \Delta v_{\text{los}} < 0 \text{ km s}^{-1}$ ). Whether D99 k-type galaxies show a similar deficit is not clear; statisti-

cal tests involving the D99 sample are not very illuminating as its small sample size generally gives inconclusive results. For example, a two-sample K-S test of the velocity distributions of all the [O II] emitters and D99 k-type galaxies with  $-2500 \text{ km s}^{-1} < \Delta v_{\text{los}} < +2500 \text{ km s}^{-1}$  gives  $\sim 92\%$  confidence that the two distributions are drawn from the same parent population. Yet, if we use the subsamples restricted spatially within the common survey area of  $-3.74 \leq \Delta \text{RA} \leq +3.97$  and  $-2.42 \leq \Delta \text{DEC} \leq +1.91$ ,<sup>7</sup> the same statistical test rejects at the 97% confidence level the hypothesis that they are drawn from the same parent distribution. At least D99 k-type galaxies do not show as pronounced a depletion near the cluster systemic velocity and might represent a virialized population; this is not a baseless assumption, since the D99 k-type galaxies appear to form a well-defined cluster red-sequence (Fig. 6), and such galaxies are likely to trace gravitationally-bound substructures (although it is almost certainly the case that Abell 851 has not been virialized over the entire cluster scale).

The biweight estimator and the jackknife method are used to estimate the velocity dispersions  $\sigma_v$  and their uncertainties (Beers et al. 1990):  $1160 \pm 140 \text{ km s}^{-1}$  and  $1010 \pm 50 \text{ km s}^{-1}$  for D99 k-type galaxies and cluster [O II] emitters, respectively. We must note, however, that Fig. 7 shows that a significant number of cluster [O II] emitters with  $\Delta v_{\text{los}} \lesssim -1000 \text{ km s}^{-1}$  escaped detection by the MLF00 narrowband search due to the sharply dropping transmission efficiency. This would lead to a severe underestimate of the true velocity dispersion for the cluster [O II] emitting population; their velocity dispersion should therefore be taken as a lower limit.

A simple kinematical treatment of infalling and virialized cluster galaxies in a cluster-scale potential leads to  $|T/V| \approx 1$  and  $|T/V| \approx 1/2$ , respectively, where  $T$  and  $V$  are the kinetic and potential energies of galaxies. In this picture, the velocity dispersions of infalling and virialized galaxies are expected to follow the relation  $\sigma_{v,\text{infall}} \approx 2^{1/2} \sigma_{v,\text{vir}}$ . Having a higher velocity dispersion compared to that of virialized cluster members therefore is often invoked as a basic attribute of an infalling galaxy population. Previous studies generally found such kinematic segregations of cluster galaxies, with star-forming galaxy populations having higher velocity dispersions (e.g., Colless & Dunn 1996; Dressler et al. 1999; Diaferio et al. 2001), although Rines et al. (2005) found little evidence for the generality of this trend using their sample of emission-dominated and absorption-dominated galaxies in virialized regions of clusters. Such disagreements only illuminate the intrinsic difficulty of minimizing the effects of biases in cluster-scale surveys of galaxies, which require a substantial amount of spectroscopy.

In short, the cluster [O II] emitters appear not to be virialized, since their velocity distribution does not follow a Gaussian around the cluster systemic velocity. Although we cannot rigorously conclude due to the small sample size of D99 galaxies, their velocity distributions restricted to the common survey area show some evidence of kinematic segregation between the cluster [O II] emitters and the D99 k-type galaxies. The non-virialized state of [O II] emitters naturally arises when they are at the infalling phase and have not spent a long time within the cluster gravitational potential.

### 3.2. Spatial Distribution

<sup>7</sup> The coordinates are given with respect to  $9^{\text{h}}42^{\text{m}}56^{\text{s}}.2$ ,  $46^{\circ}59'12''.0$  (J2000).



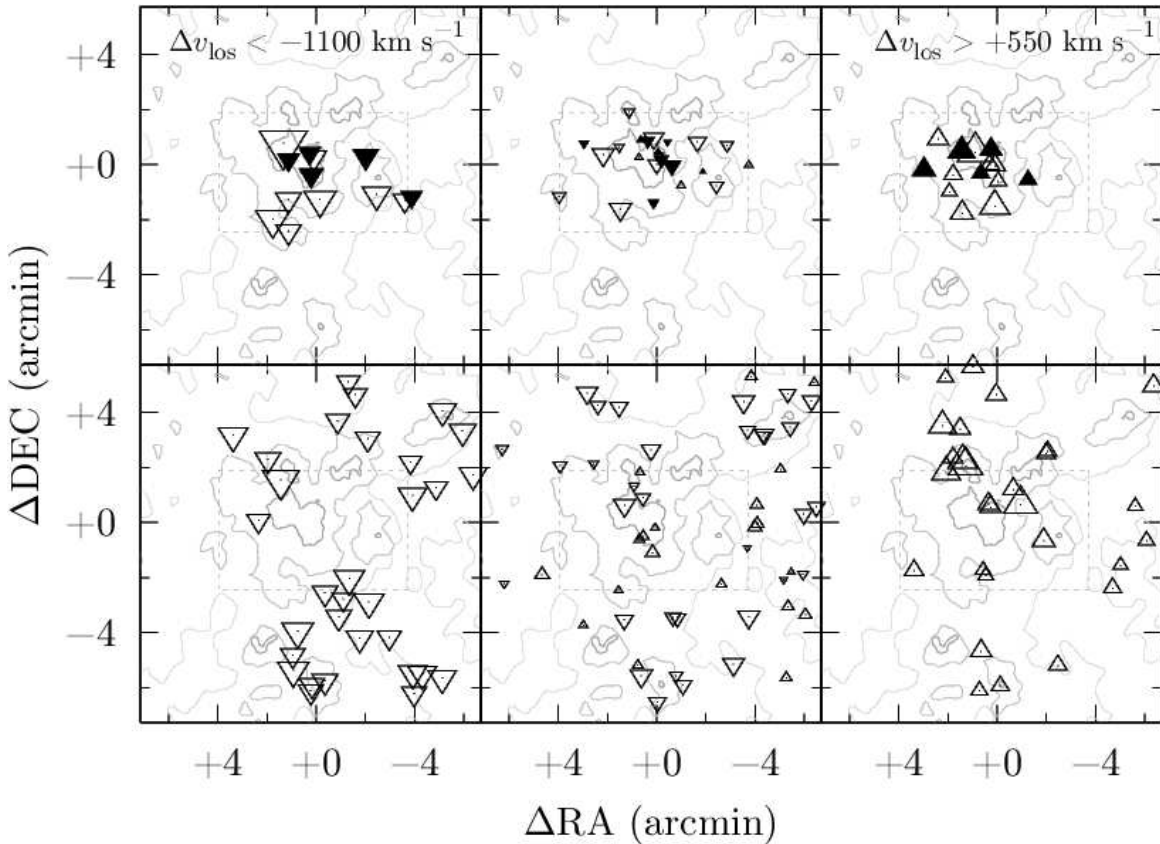


FIG. 8.— Spatial distributions of cluster [O II] emitters (*bottom row*) and D99 galaxies (*top row*) with k- (open triangles) and k+a/a+k-type (filled triangles) spectrum. Lack of D99 galaxies beyond the area enclosed by a gray dashed box is due to the smaller survey area of D99. The gray contours indicate the local galaxy densities at 5, 50, and 150  $\text{Mpc}^{-2}$  computed from K01 cluster members. In the columns the galaxies are binned by their velocity:  $\Delta v_{\text{los}} < -1100 \text{ km s}^{-1}$  (*left*),  $-1100 \text{ km s}^{-1} < \Delta v_{\text{los}} < +550 \text{ km s}^{-1}$  (*middle*), and  $\Delta v_{\text{los}} > +550 \text{ km s}^{-1}$  (*right*). Upright and inverted triangles denote redshift ( $\Delta v_{\text{los}} > 0 \text{ km s}^{-1}$ ) and blueshift ( $\Delta v_{\text{los}} < 0 \text{ km s}^{-1}$ ) with respect to the cluster systemic velocity, respectively. The symbol size is roughly proportional to  $|\Delta v_{\text{los}}|$ .

Fig. 8, on the other hand, shows clear evidence for a kinematic segregation in terms of spatial distributions of the cluster [O II] emitters and D99 k-type galaxies. In contrast to D99 k-type galaxies, [O II] emitters are only sparsely distributed in the dense, cluster core region; there are very few [O II] emitters inside or near the contour of the highest local galaxy density. This trend holds true in all the velocity bins in the figure. In Fig. 1 we have shown that the [O II] emitter fraction is a strong function of local galaxy density, and Fig. 8 only visualizes the well-established empirical relation. In wide-field imaging of Abell 851, the red-sequence galaxies are shown to trace similar large-scale structures and substructures as observed via the photometric redshift technique (Kodama et al. 2005), so it is of no surprise that the D99 k-type galaxies are found abundantly in dense regions.

The very skewed distribution of blueshifted ( $\Delta v_{\text{los}} < 0 \text{ km s}^{-1}$ ) [O II] emitters is also evident in the southern ( $\Delta \text{RA} \simeq +0'$  and  $\Delta \text{DEC} \simeq -6'$ ) and north-western regions ( $\Delta \text{RA} \simeq -4'$  and  $\Delta \text{DEC} \simeq +4'$ ). Systematically redshifted [O II] emitters are present just in the north of the cluster central region as well. Abell 851 is known for the supposed filamentary structures extending out from its central region in these directions (K01). The skewed distribution of  $\Delta v_{\text{los}}$  indicate the [O II] emitters are part of infalling substructures, especially when spatially clustered as seen clearly in the figure.

In short, we find that the cluster [O II] emitters tend to avoid the densest environments, but their skewed velocity and spatial distributions strongly suggest they are moving systemat-

ically with respect to the cluster dynamical center. Some of the spatially non-clustered [O II] emitters may be field interlopers.

### 3.3. Infalling or Backsplash Population?

True positions of the galaxies relative to the cluster cannot be determined from their redshift alone, however, and in addition to the possibility of seeing field interlopers, even cluster members beyond the virial radius ( $R_{\text{vir}}$ ) could also have gone through the cluster central region once or more in the past, constituting a so-called backsplash population (Balogh et al. 2000; Mamon et al. 2004). According to the numerical simulations, about half of the galaxies within  $1 < R/R_{\text{vir}} < 2$  can belong to a backsplash population by the present epoch,  $z = 0$ . The backsplash scenario has been invoked to explain the presence of H I deficient galaxies beyond virial radii of nearby galaxy clusters, where the galaxies appear to be ram-stripped of their H I supplies during the passage through dense intra-cluster gas of cluster cores (Solanes et al. 2002; Sanchis et al. 2002). Since the inferred physical mechanisms that transform cluster galaxies vary for infalling and backsplash populations, finding their dynamical state helps constraining SFHs of cluster galaxies.

The simulations carried out by Gill et al. (2005) have shown that backsplash and infalling populations exhibit kinematically distinct velocity distributions beyond virial radii, where a backsplash population has about a factor of two smaller cluster-centric velocities than infalling satellites. They have also shown that the distribution of cluster-centric line-of-sight

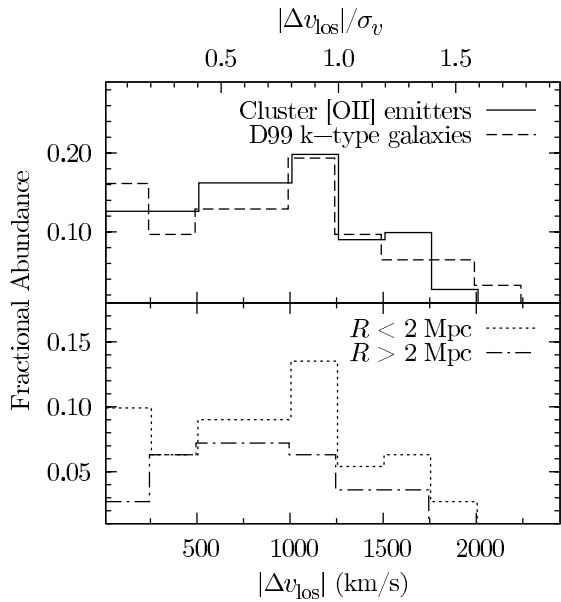


FIG. 9.— (Top) Distribution of  $|\Delta v_{\text{los}}|$  for cluster [O II] emitters (solid histogram) and D99 k-type galaxies (dashed histogram). The top axis shows the velocity normalized to an estimate of cluster velocity dispersion  $\sigma_v = 1260 \text{ km s}^{-1}$ . The fractional abundance is normalized to the total number of galaxies within each sample to facilitate comparison. Lack of low- $|\Delta v_{\text{los}}|$  galaxies is a signature of infalling population (cf., Fig. 8 of Gill et al. 2005). We note that the samples are not restricted to  $1 < R/R_{\text{vir}} < 2$ . (Bottom) The velocity distributions of the cluster [O II] emitters inside (short-dashed) and outside (dash-dotted) the fiducial virial radius of 2 Mpc. The center of the cluster was taken to be at  $9^{\text{h}}43^{\text{m}}03^{\text{s}}.3$ ,  $46^{\circ}59'26''.5$  (J2000), the brightest point in X-ray surface brightness from De Filippis et al. (2003).

velocities like Fig. 7 could imply the presence or absence of a backsplash population. Along this line, we show Fig. 9 to facilitate a comparison to Fig. 8 of Gill et al. (2005). The depletion of low- $|\Delta v_{\text{los}}|$  [O II] emitters shows quite a remarkable similarity to the distribution expected of an infalling population in their simulation. It should also be noted that unlike Fig. 8 of Gill et al. (2005) the sample used in the top figure is not restricted to those within the projected radii of  $1 < R/R_{\text{vir}} < 2$ , where the difference would be more pronounced between backsplash and infalling populations. In the same figure, the D99 k-type galaxies also appear to show a peak at a higher velocity, the signature distribution of infalling population, just as the cluster [O II] emitters do. However, we believe there are important differences, since the D99 k-type galaxies are drawn from a much smaller field of view (Fig. 8), are significantly brighter (Fig. 6), and are not necessarily representative in a statistical sense without applying proper corrections (Poggianti et al. 1999). We also lack D99 galaxies at large projected cluster radii. Furthermore, the peak around  $|\Delta v_{\text{los}}| \simeq 1000 \text{ km s}^{-1}$  do not appear to indicate a real overabundance of *general* galaxy population around that velocity, since they are not spatially coincident; see Fig. 7 for the cluster central region sample. For these reasons, we believe the depletion of low- $|\Delta v_{\text{los}}|$  galaxies is robust for the cluster [O II] emitters, yet the small sample size limits our ability to interpret the distribution of D99 k-type galaxies.

In the bottom of Fig. 9, we show the velocity distributions of [O II] emitters inside and outside the fiducial cluster virial radius of 2 Mpc, the latter enabling a more direct comparison to the Gill et al. simulations. We caution that the distributions shown here are rather sensitive to the choice of the fiducial virial radius, since the projected distribution of the cluster [O II] emitters are highly inhomogeneous as discussed earlier.

Recently both Rines et al. (2005) and Pimblet et al. (2006) carried out similar comparisons using composite galaxy samples from nearby clusters, finding galaxies in infall regions are a mixture of infalling and backsplash populations. Since the Gill et al. results are for massive, moderately relaxed clusters at  $z \sim 0$ , these works produced more direct comparisons. In contrast to these authors' findings, the “peaks” of the velocity distributions of our cluster [O II] emitters extend toward higher velocities up to  $|\Delta v_{\text{los}}|/\sigma_v \simeq 1$ , whereas the galaxies in both Rines et al. and Pimblet et al. show a steep decline in numbers at  $|\Delta v_{\text{los}}|/\sigma_v > 0.5$ . For the  $R > 2$  Mpc sample, we also observe a more pronounced depletion of low- $v_{\text{los}}$  [O II] emitters. These trends imply that the total [O II]-emitting population is probably a mixture of infalling and backsplash populations, yet the velocity distributions are generally broadened toward higher velocities than observed in local clusters, favoring a higher abundance of infalling objects.

In short, although the survey area of our spectroscopic sample is not as large as some of the most recent wide-field studies of galaxy clusters, e.g., Treu et al. (2003) and Moran et al. (2005) go out to radii of  $\sim 5$  Mpc in CL0024+1654, the analysis of their kinematics suggests that a significant fraction of the cluster [O II] emitters are likely to be still in the infalling phase.

#### 4. CLASSIFICATION BY SPECTRAL TYPE

To probe transformation of galaxy properties, we need observable indicators that are sensitive to the age of underlying stellar population. Classifying galaxies in terms of [O II]-H $\delta$  equivalent width plane is one way to put galaxies in the context of evolutionary sequence and has been used in literature (e.g., Dressler et al. 1999; Balogh et al. 1999). The equivalent widths of [O II] emission and H $\delta$  absorption, respectively, are sensitive to the on-going star-forming activity and the presence of intermediate-age stars, i.e., A- and early F-type star populations which live up to  $\sim 1.5$  Gyr with characteristically strong Balmer absorption lines. In the conventional interpretation of post-starburst galaxy spectra, the presence of strong Balmer absorption lines signals the recent cessation within the past  $\sim 1.5$  Gyr of star-forming activity after which the intermediate-age stellar population makes a dominant contribution to the integrated optical/UV galaxy spectrum. Therefore, the [O II]-H $\delta$  plane and its variants have been useful for classifying a galaxy spectrum in relation to some mechanisms which halt or significantly reduce the amount of star-forming activity within a galaxy in its recent past.

##### 4.1. D99 Spectral Class Definitions

We adopt the D99 spectral classification scheme to study the SFHs of cluster [O II] emitters (Table 1).<sup>8</sup> We stress that by convention the measured H $\delta$  equivalent width in the [O II]-H $\delta$  plane is the sum of emission and absorption equivalent widths. This means that  $W_0(\text{H}\delta) < 0 \text{ \AA}$  does not mean the line is totally seen in emission; it merely means the strength of emission equivalent width is greater than that of absorption at H $\delta$ . Although we could separate the emission and absorption components at H $\delta$  in many cases, we followed the conventional index definition to facilitate comparisons to literature. We used the equivalent widths measured using the flux-summing method for spectral indices (Paper I). We now briefly review the conventional interpretation of each spectral

<sup>8</sup> For a few objects the [O II] $\lambda$ 3727 or H $\delta$  line moved out of observed spectral range, in which case their spectra were classified into “N/A”-type.



TABLE 1  
D99 SPECTRAL CLASSIFICATION

Spectral Class	Definition		Cluster [O II] Emitters	
	$W_0([\text{O II}])$ (Å)	$W_0(\text{H}\delta)$ (Å)	$N(S/N > 2)^a$	$N(\text{all})^b$
e(b)	$< -40$	$< +4$	3	23
e(c)	$-40 - -5$	$< +4$	14	29
e(a)	$< -5$	$> +4$	40	53
k+a/a+k	$> -5$	$> +3$	2	4
k	$> -5$	$< +3$	1	2

NOTE. — The spectral indices  $W_0([\text{O II}])$  and  $W_0(\text{H}\delta)$  are measured with the flux-summing method (Paper I).

<sup>a</sup> The number of cluster [O II] emitters for which the classification is done with the equivalent width measurements at  $S/N > 2$ .

<sup>b</sup> The number of cluster [O II] emitters with each classification from the full sample.

class. For more detail, readers are referred to the original papers by D99 and Poggianti et al. (1999).

*e(b)-type.*—Galaxies in this class have a strong [O II] emission, indicative of vigorous on-going star-forming activity. Low-lying recombination lines of the Balmer series may also be seen in emission. The duration of a starburst cannot be longer than about a few 100 Myr, however, since after that timescale the buildup of continuum flux near the line decreases the [O II] emission equivalent width to a degree that the spectrum would be classified into e(c)-type.

*e(c)-type.*—Typical e(c) galaxies are a star-forming galaxy with only a moderate star-forming activity at a relatively constant rate. Local late-type spirals typically fit in this category.

*e(a)-type.*—Typical galaxies in this class have strong Balmer absorption lines as well as moderate to substantial [O II] $\lambda 3727$  emission. Based on the comparison with a local sample and high degree of dust extinction implied by low [O II]/ $\text{H}\alpha$  line ratios, Poggianti & Wu (2000) have associated typical e(a)-type galaxies to dusty starburst galaxies in which the light from the youngest starbursting population is much more extinguished than that from the intermediate to old age stellar populations (see also Poggianti et al. 2001).

*k+a/a+k-type.*—So-called post-starburst galaxies (also called E+A or  $\text{H}\delta$ -strong galaxies) with little or no [O II] emission and strong Balmer absorption lines belong to this class. This class of galaxies is often studied as a missing link between passively-evolving galaxies in clusters and actively-star-forming galaxies abundantly observed outside clusters.

*k-type.*—Passively evolving, non-star-forming galaxies like local ellipticals belong to this class. A typical k-type spectrum is dominated by the light from K-type star population, hence the designation.

A few representative spectra, actually observed in our spectroscopic survey, are shown in Fig. 10 with their corresponding D99 spectral class. Table 1 also lists the numbers of cluster [O II] emitters in each spectral class. As expected, most [O II] emitters belong to one of the emission-line classes [i.e., e(b), e(a), and e(c)], but six objects, all of which do show weak [O II] emission, are classified into non-emission-line classes. By making a cut at  $W_0([\text{O II}]) > -5$  Å, the D99 classification scheme does not strictly remove the contamination of emission-line objects into their “passive” classes. Among the four k+a/a+k type objects, three are strong Balmer-absorption systems with residual [O II] emission. One of the two k-type objects appears to have an early-type galaxy spectrum but also has [O II] and Balmer emission lines. The remaining two ob-

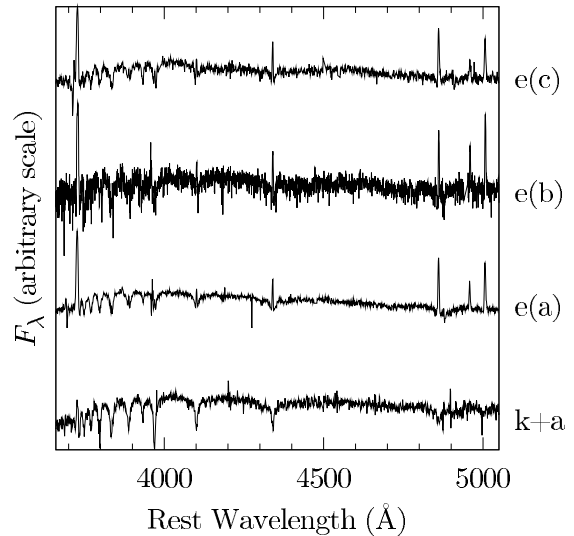


FIG. 10.— A set of observed high-S/N spectra classified into each D99 spectral class. The regions affected by very poor sky subtractions are masked from each spectrum in this figure. Note that a bright skyline and telluric absorption lines generally contaminated redshifted  $\text{H}\beta$  absorption continua, substantially increasing the uncertainties in the  $\text{H}\beta$  line flux measurements.

jects appear genuine ambiguous classifications due to poor-S/N spectra.

#### 4.2. Distribution of [O II] Emitters by Spectral Class

For our sample of cluster [O II] emitters, the limiting rest-frame [O II] equivalent width is  $\simeq -8$  Å at  $i \simeq 23$ , so there are few galaxies of k- or k+a/a+k-type, which must have  $W_0([\text{O II}]) > -5$  Å by definition; most [O II]-selected galaxies belong to one of the emission-line galaxy types: e(b)-, e(c)-, and e(a)-types. In Fig. 11 we show the distribution in the [O II]- $\text{H}\delta$  plane for Abell 851 cluster [O II] emitters with  $W_0([\text{O II}]) < -8$  Å and  $i < 23$ . To see how the distribution compares to “field” [O II] emitters, we measured the same spectral indices using the fourth data release of the Sloan Digital Sky Survey (SDSS; Adelman-McCarthy et al. 2006), the Canada-France Redshift Survey (CFRS; Lilly et al. 1995; Hammer et al. 1997), and data release one of the DEEP2 Galaxy Redshift Survey.<sup>9</sup> For each survey, we only included galaxies with  $W_0([\text{O II}]) < -8$  Å to compute the relative abundances of spectral types. Table 2 summarizes the basic characteristics of the samples. The typical size of the cluster [O II] emitters is  $2''$ – $3''$  ( $\simeq 13$  kpc at  $z = 0.4$ ), observed with  $1''$ -width slit in our spectroscopic program. The spectroscopic apertures in SDSS ( $3''$  diameter fiber), CFRS ( $1''$ – $75''$  width slit), and DEEP2 ( $1''$ -width slit) sample the regions of galaxies roughly within 5–6 kpc,  $> 11$  kpc, and  $> 8$  kpc, respectively, at the median redshift of each survey. Although we do not make an attempt to correct for the differences, the regions sampled by the surveys are comparable or at least greater than our spectroscopic aperture. All the surveys are magnitude-limited to different depths, so field samples can only be constructed to a depth brighter than the completeness limit of the cluster [O II]-emitting sample.

We constructed rough volume-limited samples by scaling the number of galaxies within similar rest-frame  $B$ -band absolute magnitudes by suitable luminosity functions from existing literature. We used software package kcorrect (v4\_1\_4; Blanton et al. 2003) to obtain absolute magnitudes from a

<sup>9</sup> <http://deep.berkeley.edu/>

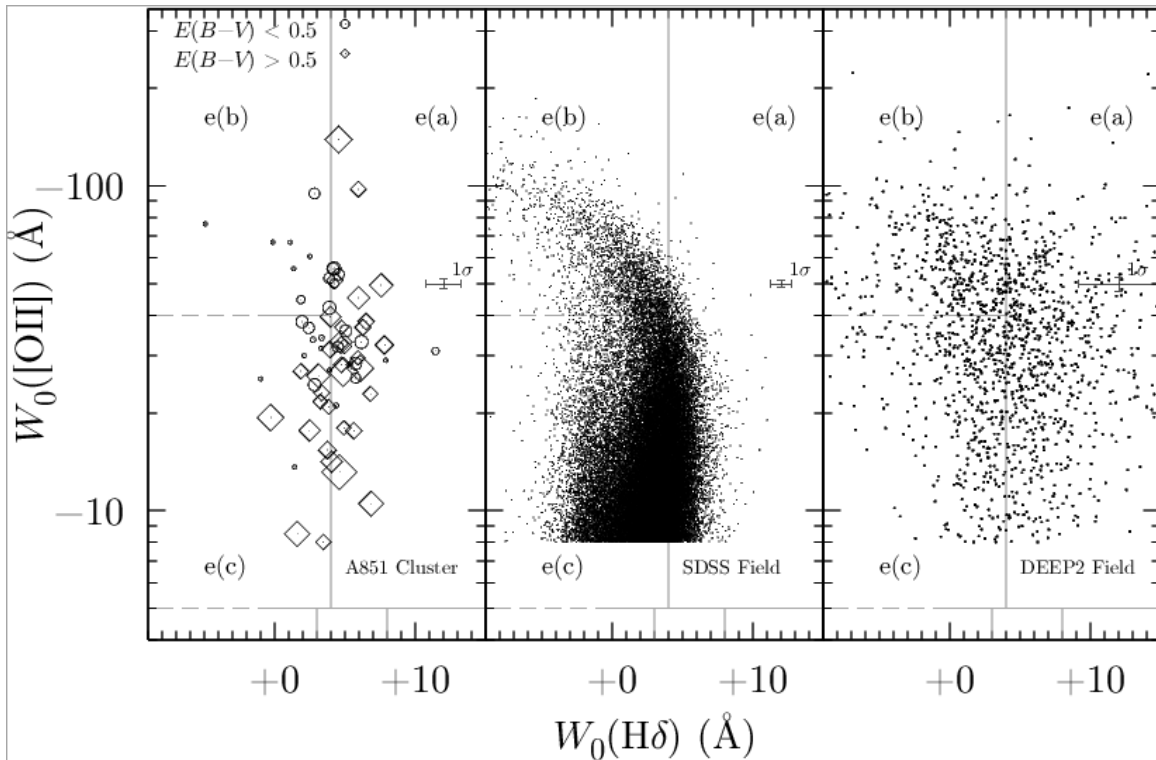


FIG. 11.— The distributions of [O II] and H $\delta$  equivalent width for  $W_0(\text{[O II]}) < -8 \text{ \AA}$  objects for magnitude-limited samples. See § 4.2 for the selection methods for SDSS and DEEP2 field samples. For the Abell 851 [O II] emitters, their reddening  $E(B-V)$  is coded by circles [ $E(B-V) < 0.5$ ] and squares [ $E(B-V) > 0.5$ ], and their size is proportional to  $E(B-V)$ . The  $1\sigma$  error bars indicate the median value for a measurement within each sample.

TABLE 2  
COMPARISON SAMPLES OF FIELD [O II] EMITTERS

Survey	$z$ Range	Magnitude Cut	Luminosity Function	Number of Spectra
SDSS (DR4) <sup>a</sup>	0.09–0.11	$i < 23^b$	Ball et al. (2005) <sup>c</sup>	41613
CFRS <sup>d</sup>	0.2–0.7	$I(\text{AB}) < 22.5$	N/A <sup>e</sup>	51
DEEP2 (DR1) <sup>f</sup>	0.8–1.0	$R(\text{AB}) < 24.1$	Willmer et al. (2005) <sup>g</sup>	1492

NOTE. — The spectral indices  $W_0(\text{[O II]})$  and  $W_0(\text{H}\delta)$  are measured with the flux-summing method (Paper I). Each field sample consists of galaxies with  $W_0(\text{[O II]}) < -8 \text{ \AA}$ .

<sup>a</sup> Only extended sources which are spectroscopically classified as galaxy with  $z_{\text{conf}} > 0.85$  are included.

<sup>b</sup> The magnitude limit of SDSS survey is  $i \approx 21.3$ ; we include fainter galaxies to increase the number of galaxies near  $M_B \approx -19$ . All photometry in our SDSS samples are Petrosian magnitudes.

<sup>c</sup> eClass PCA bivariate luminosity function (their Fig. 5). Within each magnitude bin and eClass range, an additional correction for the fraction of galaxies with  $W_0(\text{[O II]}) < -8 \text{ \AA}$  is applied to remove the contribution to the luminosity function from non-emission-line galaxies.

<sup>d</sup> Only objects with their confidence class 0–4 (Le Fevre et al. 1995) are included. As the CFRS spectra were obtained at considerably different spectral resolutions ( $40 \text{ \AA}$ ) than other surveys ( $\sim 3 \text{ \AA}$  for SDSS and  $\sim 1 \text{ \AA}$  for DEEP2), we used slightly different windows of  $3653 \text{ \AA} - 3706 \text{ \AA}$ ,  $3706 \text{ \AA} - 3748 \text{ \AA}$ , and  $3748 \text{ \AA} - 3801 \text{ \AA}$  ([O II]) and  $4030 \text{ \AA} - 4078 \text{ \AA}$ ,  $4078 \text{ \AA} - 4126 \text{ \AA}$ , and  $4126 \text{ \AA} - 4170 \text{ \AA}$  (H $\delta$ ) for the blue continuum, line, and red continuum, respectively.

<sup>e</sup> No attempts have been made to correct the sample using a luminosity function.

<sup>f</sup> Only objects with  $z_{\text{quality}} \geq 3$  are included.

<sup>g</sup> Schechter function for blue galaxies (their Table 4).

set of available broadband photometry (corrected only for Galactic extinction) for each galaxy survey. The cluster [O II] emitters near the MLF00 narrowband survey limit have  $M_B(\text{Vega}) \simeq -17.5$  (before correcting for internal extinction). Since the completeness severely decreases toward that magnitude, we limited our comparisons roughly to the survey limit of our DEEP2 sample,  $M_B < -19$ ; for both the SDSS and DEEP2 samples, the rough completeness limit in terms of absolute magnitude is  $M_B \sim -21$ , so the uncertainties in galaxy

fractions increase significantly toward the faint end of luminosity function for that reason. We caution that the above procedure was not followed for the CFRS sample because of limited availability of photometric data and significantly lower-resolution spectra; thus the CFRS data points should only be used for a rough comparison. We further note that using purely magnitude-limited samples did not significantly change the overall trends to be discussed now.

Looking at the SDSS field sample in the [O II]-H $\delta$  plane

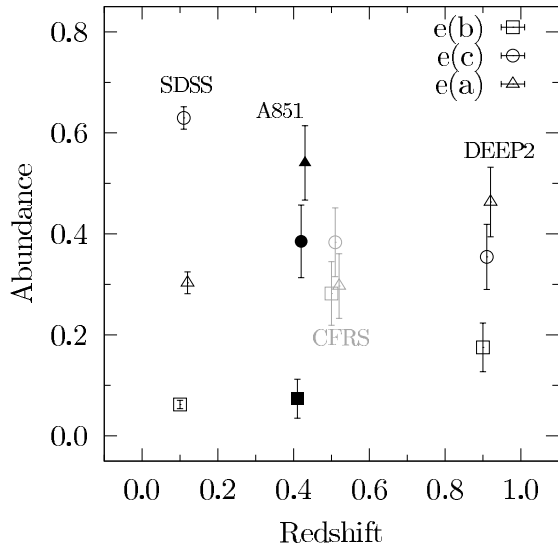


FIG. 12.— Fractional abundance of each D99 spectral class relative to all  $W_0([\text{O II}]) < -8 \text{ \AA}$  galaxies in each survey. Filled symbols denote the Abell 851 [O II] emitters. Each sample is shown roughly at its median redshift with a slight offset for clarity.

is illuminating because of its large sample size and relatively small measurement uncertainties. We notice the distribution is dominated by typical star-forming galaxies [e(c)], with relatively small pure starbursting population [e(b)]. The galaxies with e(a)-type spectrum appear to form some extension, toward stronger  $\text{H}\delta$  absorptions, of general star-forming galaxy population with e(c)-type spectrum. The DEEP2 field sample generally suffers from large uncertainties; the distribution of galaxies with low [O II] equivalent width does not appear to extend well down below  $\sim -10 \text{ \AA}$  in contrast to the SDSS sample, which indicates more vigorous star-forming activity expected of galaxies at high redshift.

In Fig. 12 we show the relative abundance of each D99 class within each sample of  $W_0([\text{O II}]) < -8 \text{ \AA}$  galaxies at different redshift. As expected, the e(b)-type galaxy fraction was higher at high redshift, reflecting the fact that triggering of young starbursts was more frequent as the universe had a greater amount of star-forming activity out to  $z \sim 2$ . A similar redshift trend is seen in the e(a)-type fractions in the field galaxy samples, but in Abell 851 the e(a) fraction is higher than or at least comparable to that in the field within the probed redshift range. It is important to note that the plot shows the fractional abundance of different spectral classes within each  $W_0([\text{O II}]) < -8 \text{ \AA}$  galaxy samples. Since the [O II] emitters constitute a progressively smaller fraction of galaxies toward lower redshift (Nakata et al. 2005), the observed trend of e(b) and e(a) galaxies in the field is stronger, if the fractions are computed within the full galaxy samples. For the same reason, the e(c) fractions within the full samples do not evolve very much in the field, if we adopt the [O II] galaxy fraction in Nakata et al. As noted earlier, e(a)-type spectrum has been attributed to dusty starburst galaxies. If this identification is true, even the e(a) galaxies constitute a starbursting population, implying that starburst phenomena in Abell 851 are at least as frequent as  $z \sim 1$  field [O II] emitters.

In computing fractional abundance of each emission-line galaxy class, we opted to take each data point in the [O II]- $\text{H}\delta$  plane as a two-dimensional Gaussian probability distribution with its best estimates and standard deviations given by the measurements of [O II] and  $\text{H}\delta$  equivalent widths and their

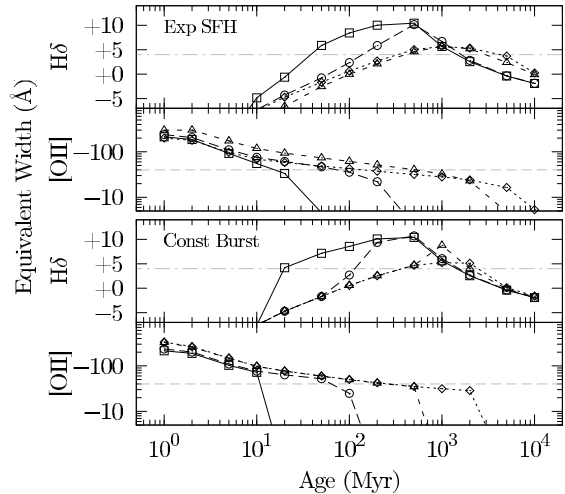


FIG. 13.— The [O II] and  $\text{H}\delta$  equivalent widths as a function of age for constant burst (bottom) and exponentially-declining SFH (top) models with the fiducial parameters  $E(B-V) = 0.5$  and  $E_*/E_g = 0.44$  (Appendix A). The models were run for star-forming timescales of  $\tau = 10 \text{ Myr}$  (solid line with square symbols),  $100 \text{ Myr}$  (dashed with circles),  $1 \text{ Gyr}$  (short-dashed with triangles), and  $2 \text{ Gyr}$  (dotted with diamonds) models. The measurements are made at the ages  $(1, 2, 5) \times (10^7, 10^8, 10^9 \text{ yr})$  and are indicated by symbols. The dashed gray line indicates the boundary of burst and non-burst populations, i.e., e(b) and e(c), as defined in terms of [O II] equivalent width. The dash-dotted gray line indicates the threshold  $[W_0(\text{H}\delta) > 4 \text{ \AA}]$  for e(a) population.

uncertainties. Each data point integrates to unity over the entire [O II]- $\text{H}\delta$  plane, but low-quality measurements give rise to some probability for each point to leak into other spectral classes than that designated solely by their best estimates. A significant number of both Abell 851 and field [O II] emitters have spectra with low S/N—about a few per pixel for Abell 851 (Paper I) and even smaller for the DEEP2 sample; by following the above procedure, we avoid giving too much confidence to the classification using the best estimates of such low-S/N measurements. Dividing the sum of integrated probabilities in each spectral class by the total number of galaxies in the [O II]- $\text{H}\delta$  plane yields the fractional abundance. For Abell 851 sample, we have taken into account the spectroscopic target selection bias by multiplying each  $g-i$  color subsample by an appropriate correction factor (Paper I).

## 5. STAR FORMATION HISTORY OF CLUSTER [O II] EMITTERS

Analyzing the cluster [O II] emitters in terms of possible evolutionary scenarios requires modeling their spectral evolution using stellar population synthesis models. The D99 spectral classification scheme employs a combination of stellar and nebular lines that are sensitive to the time evolution of galaxy spectra over a wide range in stellar age. Hence our spectral modeling considers the time evolution of synthetic spectra of underlying stellar populations as well as corresponding nebular emission. Furthermore, combining these two components enabled us to incorporate the effect of differential dust extinction on stellar and nebular components, which appears essential for reproducing e(a) spectrum (Poggiati et al. 2001). The detail of our modeling scheme is outlined in Appendix A.

### 5.1. Time Evolution in the [O II]- $\text{H}\delta$ Plane

The [O II] emitters with e(a)-type spectrum make up a significant fraction of the cluster [O II] emitters (Fig. 11), so we place an emphasis on reproducing the e(a)-type spectrum for its dominance in our sample. We immediately excluded in-

stantaneous burst models, which were also modeled, as they generally fail to reproduce a typical  $e(a)$  spectrum with strong  $H\delta$  absorption and  $[O II]$  emission at the same time. The values  $E(B-V) = 0.5$  and  $E_*/E_g = 0.44$  are chosen as fiducial numbers representing our  $[O II]$  emitting sample.

In Fig. 13 we show the evolution of  $[O II]$  and  $H\delta$  equivalent widths of constant burst and exponentially-declining SFH models. The  $H\delta$  equivalent width cut for  $e(a)$ -type galaxies is indicated by the horizontal dash-dotted lines. Strong  $H\delta$  absorption is generally achieved by the models with a shorter star-forming timescale,  $\tau \lesssim 100$  Myr, and the phase can continue up to a few Gyr, roughly comparable to the lifetime of intermediate age stellar population. These short- $\tau$  galaxies are generally classified into  $e(b)$ -type for up to  $\sim 100$  Myr during which they show strong  $[O II]$  emission ( $< -40 \text{ \AA}$ ), while their  $H\delta$  absorption has not had a time to grow as much. After the vigorous star formation, the short- $\tau$  galaxies go into a post-starburst ( $k+a/a+k$ ) phase rather quickly due to their fast fading  $[O II]$  emission. Therefore short- $\tau$  models with the fiducial parameters of  $E(B-V)$  and  $E_*/E_g$  are unlikely to explain the abundance of  $e(a)$ -type galaxies in our sample (Fig. 11), since the short- $\tau$  models stay in the  $e(a)$  phase for no more than  $\sim 100$  Myr.

Strong  $[O II]$  emission and  $H\delta$  absorption equivalent widths are achieved for a more extended duration by the models with star-forming timescales  $\tau \sim 1$  Gyr. A major difference between the constant burst and exponentially-declining SFHs with similar  $\tau$  is how star formation continues after  $t \simeq \tau$  (which characterizes roughly the ‘‘burst’’ duration). Since O- and B-type stars can totally dominate the light from a galaxy when present, the  $H\delta$  absorption line grows substantially only after a significant amount of O- and B-type stars are gone. Since star formation totally ceases after a burst, the  $[O II]$  emission equivalent width from constant burst models quickly goes below the boundary for emission-line galaxies [ $W_0([O II]) > -5 \text{ \AA}$ ] after a few Myr. On the other hand, the  $\tau \sim 1$  Gyr models with an exponentially-declining SFH can spend up to several Gyr within the emission-line categories, which is desirable for reproducing a high abundance of  $e(a)$  galaxies.

Now, Fig. 14 illuminates the effect of dust extinction in the  $[O II]$ - $H\delta$  plane with a set of  $\tau \sim 1$  Gyr exponentially-declining SFH models. A range of reddening  $E(B-V) = 0.0$ – $1.5$  roughly spans the spread of  $[O II]$  emitters. We point out that the equivalent width is a measurement insensitive to the presence of dust reddening when the continuum and line flux are both attenuated by the same amount, in which case the model tracks do not deviate from the dust-free,  $E(B-V) = 0$  model. Therefore we introduced the effect of differential extinction by varying  $E_*/E_g$ , the ratio of  $E(B-V)$  in stellar to nebular component. It is clear that differential extinction is essential for pushing a model track into the  $e(a)$  regime, as the  $H\delta$  equivalent width for the dust-free track turns over at  $\simeq 4 \text{ \AA}$ , barely crossing the boundary for the  $e(a)$  phase; taking  $E_*/E_g < 1$  extinguishes the nebular  $H\delta$  emission more than the stellar continuum around it, enabling the equivalent width to grow slightly larger in absorption (i.e., less emission filling).

However, the  $[O II]$  emission, being a bluer line, suffers even more significantly from dust extinction as well. This in turn leads to a degeneracy between the age and the amount of reddening in the  $[O II]$ - $H\delta$  plane. For example, a highly reddened  $E(B-V) = 1.5$  starbursting galaxy at the age of 100 Myr is hard to distinguish from a  $E(B-V) = 0.5$  galaxy

TABLE 3  
 $i$ - $\log \Sigma$  SUBSAMPLES

Category	$\log \Sigma$	$i$	$N$
HB	$> 1.6$	$< 21$	10
TB	$0.0 - 1.6$	$< 21$	3
LB	$< 0.0$	$< 21$	6
HM	$> 1.6$	$21 - 23$	14
TM	$0.0 - 1.6$	$21 - 23$	29
LM	$< 0.0$	$21 - 23$	6
HF	$> 1.6$	$> 23$	6
TF	$0.0 - 1.6$	$> 23$	19
LF	$< 0.0$	$> 23$	11

at  $\sim 3$  Gyr, since they both would have  $W_0([O II]) \simeq -11 \text{ \AA}$  and  $W_0(H\delta) \simeq 5 \text{ \AA}$ . The inferred age of star-forming activity can be quite different without the knowledge of reddening for breaking such a degeneracy.

### 5.2. Star Formation History by Composite Spectra

We recall that it was largely the interpretation of low-S/N  $H\delta$  equivalent width measurements which led to the controversy regarding the frequency of starbursts in cluster galaxies (Dressler et al. 1999; Balogh et al. 1999). Although our analysis of  $e(a)$ -type galaxies in the  $[O II]$ - $H\delta$  plane in the previous section independently confirms the high abundance of cluster galaxies with strong Balmer absorption lines, also reported recently by Dressler et al. (2004), the relatively low spectral S/N of faint  $[O II]$  emitters limits our ability to constrain the individual SFHs with much confidence. For our typical spectra, a  $3\sigma$  detection of  $H\delta$  absorption equivalent width at  $W_0(H\delta) \sim 5 \text{ \AA}$ , for example, needs per pixel S/N  $\sim 10$  in the continuum, a requirement not quite met by most of our spectra (Sato & Martin 2006). We therefore supplement our analysis by composite spectra, which smear out the SFHs of individual galaxies but would help us find the characteristic SFHs of subsamples.

Our scheme for subsampling cluster  $[O II]$  emitters is motivated by the observational evidence that the transformation of galaxies depends both on their intrinsic property and on their local environment. We chose  $i$  magnitudes and local galaxy densities  $\Sigma$  to characterize these attributes; Fig. 5 shows the classification scheme, and Table 3 shows the number of objects within each subsample. We effectively make subsamples residing in the local environments characteristic of low-density, field-like regions (L;  $\log \Sigma < 0.0$ ), the transitional zone (T;  $0.0 < \log \Sigma < 1.6$ ), and the high-density regions (H;  $\log \Sigma > 1.6$ ). The highest density cut was made close to the K01 threshold density. Each density bin is further divided into three  $i$  magnitude bins: bright (B;  $i < 21$ ), medium (M;  $21 < i < 23$ ), and faint (F;  $i > 23$ ). The subsampling yields composite spectra of quality ranging from per pixel continuum S/N  $\sim 3$  for faint subsamples to S/N  $\sim 30$  for bright subsamples. For faint subsample this is still an improvement, as most  $i > 23$   $[O II]$  emitters have S/N  $< 2$ .

The goal of this exercise is to study the SFHs inferred from representative composite spectra of various cluster  $[O II]$ -emitting subsamples by placing them in the  $[O II]$ - $H\delta$  plane. For this reason the method for coadding spectra must not artificially change the resulting  $[O II]$  and  $H\delta$  equivalent widths of composite spectrum, i.e., continuum flux strength relative to the line flux must be scaled properly at these lines. Averaging spectra normalized to a common mean flux density over a relatively featureless continuum region for the entire spectrum is not desirable, especially for  $[O II]\lambda 3727$ , since the emission

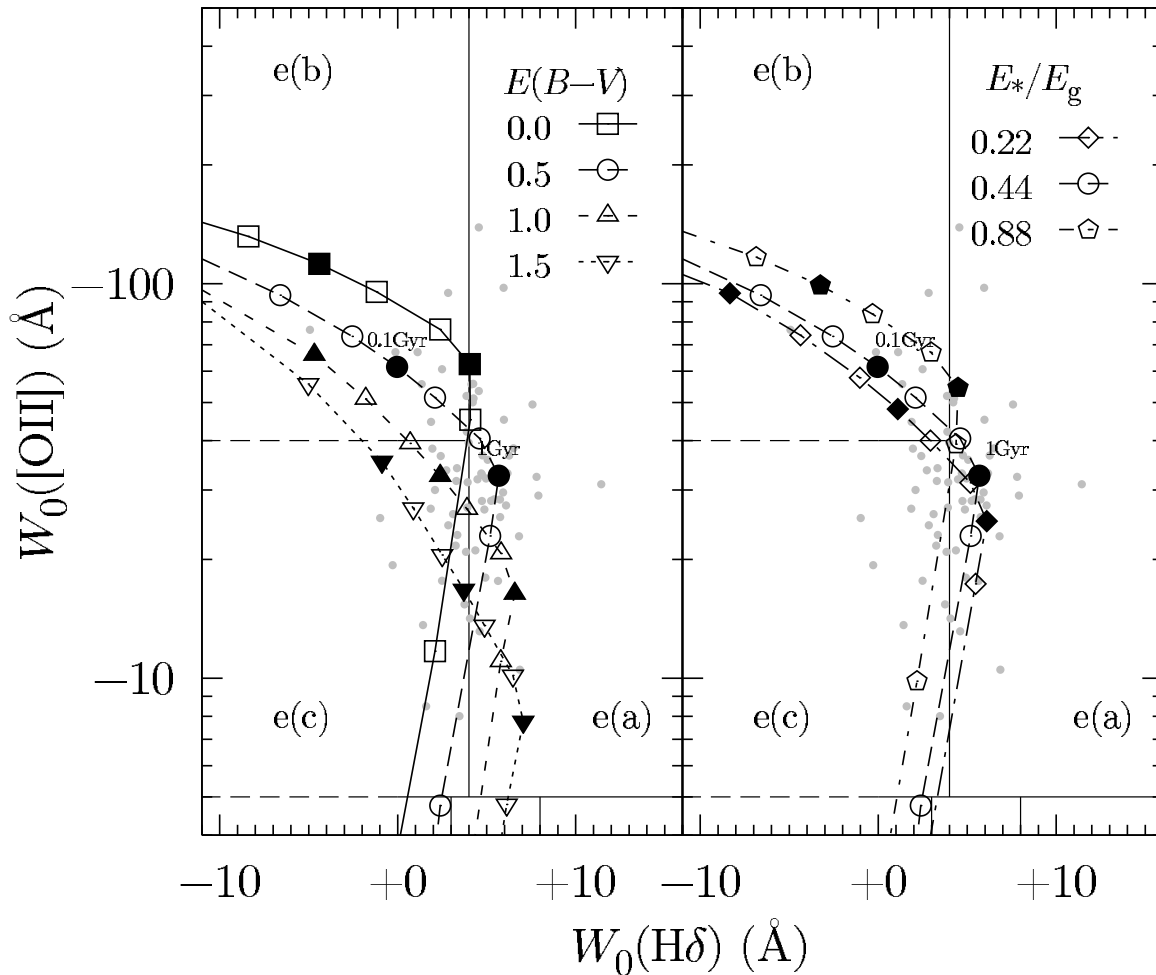


FIG. 14.— The effect of dust extinction on the observed spectral indices of a fiducial model track (exponentially-declining SFH with  $\tau = 1$  Gyr,  $E(B-V) = 0.5$ , and  $E_*/E_g = 0.44$ ) indicated by circles connected by dashed line. (Left) The output spectra from the model were extinguished by a different amount of  $E(B-V)$  at constant  $E_*/E_g = 0.44$ . (Right) Stellar and nebular continua were differentially extinguished at a ratio given by  $E_*/E_g$  at constant  $E(B-V) = 0.5$ . Filled gray circles indicate models at 10 Myr, 100 Gyr, and 1 Gyr. Filled gray circles are observed cluster [O II] emitters.

line appears within a sloping continuum region of the Balmer break. Instead we normalized spectra to the continuum flux density at line center of each line of interest, after the spectra are shifted to their rest frame wavelengths. All spectra are rebinned to a common dispersion at  $1 \text{ \AA}$  per pixel before averaging to produce the final composite spectrum. A potential bias may be introduced to a composite spectrum depending on how each spectrum is weighted or not weighted against others within the common subsample. We cannot weight by such quantities as inverse variance, since it is strongly dependent on source luminosity, an intrinsic property of subsample population which we wish to control. In order to treat each [O II] emitter within a subsample on equal footing, the composite spectrum was computed without weighting. The results are also checked against the composite spectra made from medianing, which is generally more robust against outliers. We also excluded objects identified to be AGN-like from our composite samples.

In Fig. 15 we see where the subsamples lie in the [O II]-H $\delta$  plane, overlaid on the evolutionary tracks of our fiducial models for  $E(B-V) = 0.0 - 1.5$ . Within similar local environments, the [O II] equivalent width of [O II] emitters is strongly dependent on their  $i$  magnitude; luminous galaxies tend to have a weaker [O II] emission, in line with what we found in Paper I. Remarkably, their H $\delta$  equivalent widths are

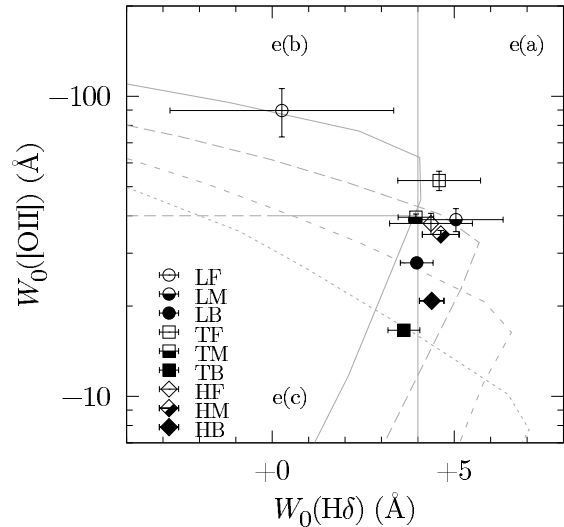


FIG. 15.— The [O II] and H $\delta$  equivalent widths from the composite spectra of  $i$ - $\Sigma$  subsamples. The  $1\sigma$  uncertainties were computed formally from the sigma vectors of spectra to be coadded. The gray lines indicate our fiducial emission galaxy models at  $E(B-V) = 0.0$  (solid),  $0.5$  (long-dashed),  $1.0$  (short-dashed), and  $1.5$  (dotted); see Fig. 14. The uncertainties in  $W_0([O II])$  for some data points are smaller than their symbol size.

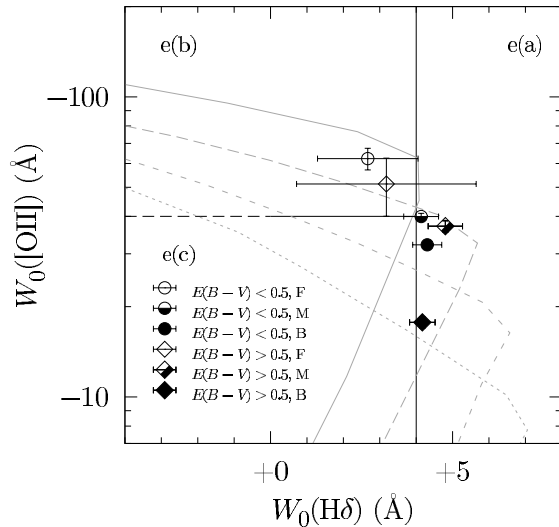


FIG. 16.— [O II] and H $\delta$  equivalent widths of the composite spectra from the  $i$ - $E(B-V)$  subsamples (§ 5.2). A cut was made at  $E(B-V) = 0.5$  to divide [O II] emitters into galaxies with low and high reddening, and each subsample was further divided into three luminosity bins with cuts at  $i = 21$  and 23. The uncertainties in  $W_0([\text{O II}])$  for some data points are smaller than their symbol size.

nearly constant at  $4-5 \text{ \AA}$ , and only the LF sample stands out with a small H $\delta$  equivalent width in absorption ( $\sim 0 \text{ \AA}$ ). The LF sample is classified into e(b)-type, yet its H $\delta$  measurement has a large uncertainty; within  $2\sigma$ , the LF data point is consistent with being e(a)-type. While this is true, it is generally difficult for a spectrum to have strong [O II] emission and H $\delta$  absorption equivalent widths at the same time because of emission filling at H $\delta$ . A very strong [O II] emitter with  $W_0([\text{O II}]) \lesssim -100 \text{ \AA}$  would always have H $\delta$  equivalent width in emission, i.e.,  $W_0(\text{H}\delta) < 0 \text{ \AA}$  (Fig. 14). Therefore, with a reasonable confidence in the very strong [O II] emission, it is likely that the LF composite galaxy is a true e(b)-type galaxy.

It appears our model tracks with  $E(B-V) = 0.0-1.5$  almost entirely cover the range of measurements from the composite spectra. While this may indeed imply the importance of dust extinction, we expect the  $i$ - $\Sigma$  sampling scheme to have degeneracy on the amount of dust reddening in the [O II]-H $\delta$  plane. Composite sampling makes more difficult to interpret the distribution seen in Fig. 15 in terms of the amount of reddening, since we have seen there is a positive trend of  $E(B-V)$  on galaxy luminosity (Paper I).

To better interpret the effect of reddening, we make another subsampling based on  $E(B-V)$  in Fig. 16. On a model evolutionary track, increasing  $E(B-V)$  has an effect of pushing the entire track toward weaker [O II]-emitting e(a)-type galaxy (Fig. 14). If the dust reddening is the primary parameter for the spread of [O II] emitters, resampling them based on  $E(B-V)$  might form a one-parameter family of data points along the evolutionary track on the [O II]-H $\delta$  plane, but we see this is not the case. A cut was made at  $E(B-V) = 0.5$  to divide [O II] emitters into galaxies with low and high reddening, and each subsample was further divided into three luminosity bins with cuts at  $i = 21$  and 23. For the subsamples with similar luminosities, the effect of reddening does not appear to be as strong as expected from the shift in the model tracks arising from varying the amount of reddening alone, except perhaps for the brightest subsamples. The general trend of decreasing strength of [O II] equivalent width with luminosity is still observed.

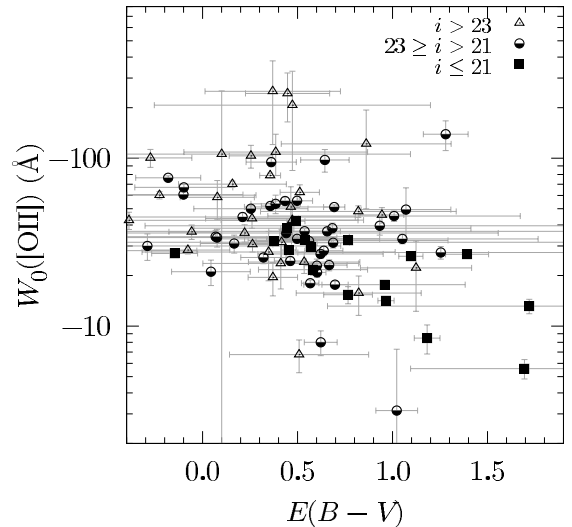


FIG. 17.— Rest-frame [O II] equivalent widths of cluster [O II] emitters as a function of their reddening  $E(B-V)$ . Data points are divided into low- ( $i > 23$ ; open triangles), intermediate- ( $23 \geq i > 21$ ; half-filled circles), and high-luminosity ( $i < 21$ ; filled squares) sources. Objects identified to be AGN-like are excluded from the figure.

The luminosity trend is particularly hard to interpret for moderate [O II] emitters in the presence of dust, since evolutionary tracks give rise to degeneracy in burst age and the amount of reddening. For example, in Fig. 16 the luminous (B),  $E(B-V) > 0.5$  subsample lies close to the point at which the model tracks with  $E(B-V) = 0.5$  and 1.5 intersect. As far as the amount of reddening is concerned, both the evolutionary tracks are very roughly consistent with the measured  $E(B-V)$ , yet the inferred burst age is very different depending on what the actual  $E(B-V)$  is— $\sim 100$  Myr for  $E(B-V) = 1.5$  and  $\sim 3$  Gyr for  $E(B-V) = 0.5$ . Rather than constructing composite samples, treating galaxies individually with distinct, more precise reddening measurements would better constrain their SFHs in this case, if the quality of spectra allows it.

To better elucidate the coupled effect of luminosity and reddening in the [O II]-H $\delta$  plane, in Fig. 17 we relate the [O II] equivalent width, luminosity, and the amount of reddening. We clearly see that luminous ( $i < 21$ ), weak-[O II] emitters [ $W_0([\text{O II}]) \sim -10 \text{ \AA}$ ] are highly reddened with  $E(B-V) \sim 1$ . The bright subsamples in Fig. 15, LB, TB, and HB, lie in the region roughly bounded both by the tracks at the age of  $\sim 1-2$  Gyr of low reddening  $E(B-V) \simeq 0.0-0.5$  model galaxy and the tracks at the age of  $\sim 100$  Myr of high reddening  $E(B-V) \simeq 1.0-1.5$  model galaxy. The observed high reddening suggests the younger, highly reddened burst is a more natural interpretation of luminous, weak-[O II] emitters. In general, we see that large amount of reddening can make young starburst galaxies appear in the same loci as less reddened starburst at older burst age, and we tend to observe them in the e(a)-type spectrum. A high amount of reddening typically observed in the cluster [O II] emitters [ $E(B-V) \gtrsim 0.5$ ] suggests that younger burst ( $\lesssim 1$  Gyr) is more likely to explain the dusty [O II]-emitting population.

## 6. DISCUSSION

Recent wide-field surveys of cluster galaxies have shown convincing evidence that the transformation of galaxy properties starts well beyond the virialized part of galaxy clusters, signaling the importance of local environments for preprocessing of cluster galaxies (e.g., Balogh et al. 1997; Treu et al. 2003; Rines et al. 2005; Moran et al. 2005; Pimblet et al.



2006). The star-forming properties of Abell 851 [O II] emitters have shown a strong dependence on local environment as often reported in literature; the [O II] emitter fraction depends strongly on local environments (e.g., Balogh et al. 2004b; Kodama et al. 2004; Nakata et al. 2005), while the strength of [O II] equivalent width is relatively independent of environment (Balogh et al. 2004a,b; Kodama et al. 2004; Rines et al. 2005). These properties in [O II] emission are consistent with the interpretation that the mechanisms that give rise to the suppression of star-forming activity either act on very short timescales or are sufficiently rare, i.e., the abundance of transient objects is relatively small. Furthermore, there appears a luminosity segregation of the [O II]-emitting populations in dense environments—at the luminous end, there is an indication that AGN activities could play a role in suppressing star-forming activity, whereas cluster [O II] emitters are notably absent at the faint end.

### 6.1. Timescales of Star-Forming Activity

We put some constraints on the timescales of star-forming activity in the cluster [O II] emitters using a combination of stellar population synthesis and nebular photoionization codes. Figures 14 & 15 show that the spread of cluster [O II]-emitters in the [O II]-H $\delta$  plane may be covered well by exponentially-declining SFH models of  $\tau \sim 1$  Gyr, with varying amount of reddening up to  $E(B-V) \sim 1.5$ . A wide range of reddening, however, gives rise to a degeneracy between the burst age and reddening—a young, very dusty starburst and a less dusty star-forming galaxy at an older stage of evolution can appear at a similar locus in the [O II]-H $\delta$  plane.

The composite spectra of the subsamples in the  $i$ - $\Sigma$  plane indicate that the galaxy luminosity is a major factor contributing to the spread of [O II] equivalent widths (Fig. 15). This is expected, since there exists an empirical anti-correlation between the [O II] equivalent width and galaxy luminosity (Paper I). The interpretation of equivalent width is somewhat complicated by the fact that it also is a measure of relative fraction in young and old stellar populations; a galaxy with a small vigorously star-forming regions spread within a much larger region of old stellar population would have a weaker [O II] emission equivalent width, for example. Our spectral modeling assumed simplistic SFHs for which 100% of galaxy mass is produced in a single episode of star formation. A more reasonable scenario involves patches of young star-forming regions embedded within older stellar populations. In such a case, both [O II] emission and H $\delta$  absorption equivalent widths from spatially integrated spectra would shift slightly toward the origin ( $W = 0$  Å) in the [O II]-H $\delta$  plane, in which the amount of shift is sensitive to the relative abundances of young and old stellar populations. Albeit modeling extreme cases, it is still encouraging that a simple treatment of differential extinction, as suggested by Poggianti et al. (2001), have reproduced the spread of observed [O II] emitters in the [O II]-H $\delta$  plane.

Fig. 11 shows among the most abundant [O II] emitters in Abell 851 and in the field at high- $z$  are those with the e(a)-type spectrum. We re-emphasize that properly taking account for the differential dust extinction in the stellar and nebular components of a galaxy spectrum is essential for interpreting the e(a)-type spectrum. The dust-free model track barely reaches the H $\delta$  absorption equivalent width strong enough to be considered an e(a)-type in Fig. 14. The identity of H $\delta$ -strong galaxies with moderate-to-strong [O II] emission has been somewhat enigmatic, since emission-filling at H $\delta$  ab-

sorption line can reduce its apparent strength seen in absorption. Although the nature of e(a) galaxies and its role in cluster galaxy evolution remain debatable, the original interpretation of e(a) galaxies as dusty starbursts by Poggianti et al. (1999) has recently been given considerable boosts. A study of SDSS galaxies at  $z \sim 0.1$  by Balogh et al. (2005) has concluded that they are normal or dusty spiral galaxies with  $E(B-V) \sim 0.7$ , assuming the Milky Way extinction of  $R_V = 3.1$ ; a recent study of mid-infrared sources also have supported the picture that e(a) galaxies are dusty starbursting systems (La Franca et al. 2004).

Although not a direct proxy for the presence of A-type stellar population, a very large positive value of H $\delta$  equivalent width must indicate a dominant A-type star contribution over optical spectrum, with the H $\delta$  emission-filling potentially masking their presence by reducing the equivalent width seen in absorption. H $\delta$ -strong galaxies have been studied extensively in the context of post-starburst/star-forming systems, since a substantial amount of young O- and B-type stars have to be gone before the intermediate-age stars can dominate the optical spectrum. The simplest SFH that produces a post-starburst/star-forming spectrum is a truncation SFH after an episode of starburst or star formation. For an e(a)-type spectrum, however, some residual star-forming activity after a burst is necessary to reproduce [O II] emission in dust-free models (Poggianti et al. 1999). Our modeling of e(a) spectra also does not favor simple truncation of star forming activity (§ 5.1).

When differential dust reddening is accounted for,  $\tau \sim 1$  Gyr models reproduce well the spread of cluster [O II] emitters in the [O II]-H $\delta$  plane. That the timescale of  $\tau \sim 1$  Gyr is of order of A-type star lifetime is not a coincidence; large H $\delta$  absorption equivalent widths simply require A- or early-F-type star populations. This brief window of order 1 Gyr during which H $\delta$  absorption is strong identifies either the recent cessation of starburst or on-going starburst. The former is the case for a post-starburst galaxy since the nebular emission fades quickly due to the absence of hot, young stars after a burst, and the latter is the case for an e(a)-type galaxy since the nebular emission lines are highly extinguished. Hence strong H $\delta$  absorption equivalent width tends to signal the presence of starburst; high reddening further implies the starburst could be younger than what dust-insensitive indicators of star formation would suggest.

Since the inferred timescales,  $\lesssim 1$  Gyr, of starburst are shorter than cluster-crossing timescales (typically a few Gyr), the higher abundance of starbursting e(a) galaxies compared to the field fraction strongly suggests the connection between enhanced star-forming activity and infalling cluster substructures, as discussed in § 3.

### 6.2. The Cause of Enhanced Star-Forming Activity

Fig. 12 compares the cluster and field [O II]-emitting samples, showing the e(a) abundance in Abell 851 is roughly at the same level as  $z \sim 1$  field galaxies among [O II] emitters. Since the e(a) fraction significantly declines from  $z \sim 1$  to  $z \sim 0.1$ , it is likely that e(a) galaxies are fractionally more abundant in Abell 851 than in the field at a similar redshift. We argue that this enhancement of cluster e(a) population is likely caused at the expense of continuously star-forming e(c)-type galaxies. First, our constraint on the burst age,  $\lesssim 1$  Gyr, of e(a) galaxies is consistent with the triggering of starburst upon cluster infall, whose timescales are on the order of a few Gyr. Although the timescale argument does not necessar-

ily prove the greater frequency of starbursts upon infall [e.g., upon infall, e(c) galaxies could drop out of the [O II]-emitting sample at a faster rate via truncation of star formation than the e(a) production rate via starburst], a higher burst fraction is consistent with post-starburst (E+A) galaxies being more abundant *within the total galaxy population* in clusters than in the field at intermediate redshifts (Dressler et al. 1999; Tran et al. 2003, 2004, but see Balogh et al. (1999)). Second, starburst galaxies almost certainly require gas-rich progenitors. The only class of galaxies with reasonably ample fuel supply is star-forming e(c) galaxies. Due to their short lifetime, e(b) galaxies would not make a significant contribution. Third, the e(c)-to-e(a) transformation appears consistent with their morphology. Poggianti et al. (1999) find e(a) and e(c) galaxies in  $z \approx 0.4$  clusters tend to show late-type disk morphology, but e(a) galaxies appear much more likely to be associated with mergers or strong interactions. Balogh et al. (2005) also find field e(a) galaxies in  $z \approx 0.1$  to show disk-dominated morphology. Furthermore, their distributions in the [O II]-H $\delta$  plane (Fig. 11) indicate e(a) galaxies are neither rare or particularly special in their properties. As clearly seen in the SDSS field sample, at least some galaxies in the e(a) class simply constitute a high-H $\delta$  extension of e(c) galaxies following an evolutionary track for a small- to moderate- $E(B-V)$ ,  $\tau \sim$  several Gyr exponentially-declining model, which is a typical SFH for spiral galaxies. Perhaps the e(a) galaxies of Balogh et al. (2005) constituted of a mixture of H $\delta$ -strong, but otherwise normal e(c)-type galaxies and real dusty disk galaxies observed during an episode of starburst. The set of evidence here naturally points to the underlying connections between e(a) and e(c) galaxies—it is reasonable that triggering of starbursts in gas-rich e(c) galaxies gives rise to e(a) galaxies in these contexts.

The process of e(c) to e(a) transformation must induce increased amount of dust in e(a) galaxies. At high redshift beyond  $z \gtrsim 0.7$ , mergers are presumably more frequent, and infrared-luminous sources appear to dominate star-forming activity (e.g., Le Flocc’h et al. 2005), implying the importance of star-forming activity obscured by dust. These observations indicate the apparent connection between dynamically active environment and its effect on inducing dusty starburst. Although major mergers are not likely to result in disk systems, merger-induced dusty starburst has been proposed as a mechanism for reproducing e(a) spectrum (Shioya & Bekki 2000); dust plays an essential role in prolonging the e(a) spectrum phase by extinguishing emission lines from star-forming regions. It is known that most vigorously star-forming galaxies emit strongly in infrared through dust reprocessing of UV light from young stars. Thus it is not surprising that e(a) galaxies are dusty, if they are in fact starburst galaxies. Furthermore, the selectively higher extinction of light from very young stellar population (Poggianti et al. 2001) would tend to yield high reddening values, if the nebular lines originating from vigorous star-forming activity can be measured at all. Our spectral evolutionary tracks assumed constant reddening  $E(B-V)$  throughout the lifetime of a starburst galaxy. If, instead, the amount of extinction has a decreasing trend with the age of the stellar population sampled for observation, the fact that e(a) galaxies are dustier just reflects the significant presence of very young stellar populations on top of underlying older stellar populations. Therefore the high reddening values favor a picture of e(a) galaxies as starbursts by inferring the presence of very young stellar populations but may not help us constrain one mechanism over others as to what

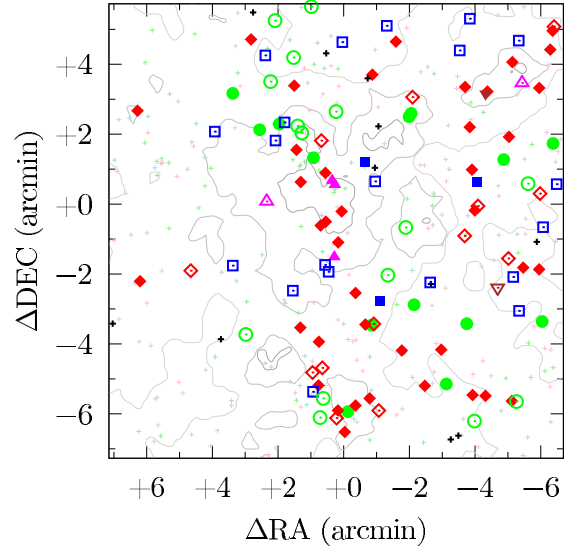


FIG. 18.— Spatial distribution of cluster [O II] emitters in terms of their D99 spectral class: e(b) (blue squares), e(c) (green circles), e(a) (red diamonds), k (brown inverted triangles), and k+a/a+k (magenta triangles). Black crosses denote [O II] emitters for which a spectral class cannot be determined. Filled symbols denote the spectral class derived from better than  $2\sigma$  measurements of line indices, whereas open symbols denote that from  $< 2\sigma$  measurements. Smaller, slightly faded crosses are MLF00 [O II] emission-line candidates not observed spectroscopically; these are  $g-i$  color-coded by blue ( $1 < g-i$ ), green ( $1 < g-i < 2$ ), red ( $g-i > 2$ ), and gray (the uncertainty in  $g-i$  is  $> 0.5$ ). The contours are the same as in Fig. 8. [See the electronic edition of the paper for a color version of this figure.]

actually causes starbursts, i.e., dusty starbursts do not *have* to be caused by mergers or interactions.

The question yet to be answered clearly is what physical mechanisms are causing the cluster [O II] emitters to go through starbursts. To address this, we see in Fig. 18 the spatial distribution of cluster [O II] emitters with their D99 spectral class. A remarkable observation is the high degree of clustering of e(a) galaxies near or inside the infalling groups, i.e., the southern and north-western clumps of galaxy overdensities, and the periphery of cluster central region. The apparent increase of galaxies showing starburst signatures in their spectra near the K01 threshold density (Fig. 3) offers another evidence for such a trend. In galaxy groups beyond the cluster virial region, both major mergers (Icke 1985; Mihos 1995; Bekki 1998) and galaxy harassment (Moore et al. 1999) are probable, but the effect of intracluster medium is expected to be less effective. Therefore galaxy-galaxy interactions offer a natural explanation for the starburst triggering mechanisms in those environments. The best way to confirm this hypothesis is to look at their morphology for signs of interactions. Some high-resolution Wide Field Planetary Camera 2 (WFPC2) images from *Hubble Space Telescope* (HST) exist for Abell 851, but unfortunately the infalling substructures seen in Fig. 18 are outside of their coverage.

Turning our attention to the cluster central region, we see e(a) galaxies residing mostly in the *periphery* of the highest galaxy-density contour (Fig. 18). Although some of these [O II] emitters could be 2D-projected foreground/background galaxies in moderately dense infall group environments along the filament outside the core, the [O II] emitters are mostly seen in the lowest velocity bin in Fig. 8, indicating their radial velocities are relatively close to the cluster systemic. In the core environment, both the intracluster gas and gravitational potential of the cluster can interact with cluster galaxies. Major galaxy-galaxy mergers are expected to be very rare, since

TABLE 4  
CLUSTER [O II] EMITTERS WITH *HST* WFPC2 MORPHOLOGY

MLF00 ID <sup>a</sup>	$\Delta$ RA <sup>b</sup> (')	$\Delta$ DEC <sup>b</sup> (')	D99 Class <sup>c</sup>	S97 ID <sup>d</sup>	Hubble Type <sup>e</sup>	D <sup>f</sup>	Interpretation <sup>g</sup>	Comment
1448	+0.76	-3.94	e(a)	<i>314</i>	Sbc	2	Tidal feature?	Face-on disk or disturbed spheroid? Shells or arms?
1640	+1.32	-3.53	e(a)	<i>2022</i>	Sb	0		Multi-armed disk galaxy; bright central disk, small bulge
2095	+1.55	-2.48	<i>e(b)</i>	<i>499</i>	Sc	1		Small, highly inclined disk; slight structure visible
2303	+0.46	-1.94	<i>e(b)</i>	<i>N/A</i> <sup>h</sup>				
2978	+0.70	-0.61	e(a)	<i>2016</i>	E	0		
3005	+0.55	-0.50	e(a)	620	Sb/S0?	1	Tidal feature?	Small, high SB spheroid; featuring disk w/arms, or tidal
3215	+0.06	-0.21	e(a)	497	Sbc	2	Merger	Visually disturbed, high SB spiral; probably merger with tail at 11
3568	+1.31	+0.63	e(a)	34	SBab	0		High SB bulge or nucleus; weak arms from bar
3600	+0.27	+0.55	k+a	122	Sd	3	Merger	Disk system with tails; bright blobs—likely merger
3604	+0.35	+0.67	a+k	36	Sd	2	Merger	Very high SB, disk object w/ 2 blobs and tail

NOTE. — First four galaxies are in Field 2 of the Smail et al. (1997) survey which sampled galaxies in the “outskirts” of Abell 851, and the latter six are from the cluster central region from the same survey.

<sup>a</sup> MLF00 object ID from their [O II] emission-line search.

<sup>b</sup> Relative to  $9^{\text{h}}42^{\text{m}}56^{\text{s}}.2, 46^{\circ}59'12''0$  (J2000).

<sup>c</sup> D99 spectral class derived from our measurements. The classification derived from  $< 2\sigma$  measurements are italicized.

<sup>d</sup> Cross-identification with Smail et al. (1997). The IDs from the pointing outside the cluster center, i.e., CI0939+47 Field 2 in their catalog, are italicized.

<sup>e</sup> The standard Hubble classification scheme (E, S0, Sa, Sb, etc.).

<sup>f</sup> Disturbance class: 0, normal; 1, moderate asymmetry; 2, strong asymmetry; 3, moderate distortion; 4, strong distortion.

<sup>g</sup> Interpretation of disturbance classes, roughly divided into (M) merger, (I) tidal interaction with neighbor, (T) tidal feature, (C) chaotic, and (!) remarkable.

<sup>h</sup> No matching object found in the morphology catalog.

the deep gravitational potential well of cluster means that the galaxies close to the cluster dynamical center are moving very fast, reducing the probability for a low-speed encounter with another galaxy. Yet galaxy harassment, in the sense of high-speed encounters between galaxies, would still be effective in the central region. The morphological analysis using *HST* has been done for many galaxies in the central region of Abell 851 by well-trained morphologists. In Table 4 we list a common subset from the catalog by Smail et al. (1997) and our [O II] emitters. Of particular interest here are those objects found within the cluster central region (the latter six in the list). Four out of six galaxies have their disturbance class greater than 0, meaning there is some morphological sign of interaction in those galaxies. Of these, three are presumably mergers, although we are not sure whether the Smail et al. interpretations distinguish between high-speed (i.e., harassment) and low-speed galaxy-galaxy encounters (i.e., major/minor mergers). As the comment indicates the remaining one is not a clear-cut case, and the cause of its disturbance is not clear.

In any case, the existing morphological data in Abell 851, though limited in quantity, indicate a high fraction of the cluster e(a) galaxies are involved in interaction. As discussed earlier, Poggianti et al. (1999) already noted a higher incidence of mergers or interactions in e(a) galaxies compared to e(c) galaxies from the full Smail et al. morphology catalog of intermediate redshift clusters. We further note that most of the [O II] emitters in the central region are morphologically classified into disk galaxies, yet their spectral signature implies a current or recent starburst. In the presence of high reddening, their optical colors and the strength of [O II] emission may not give an obvious indication of starburst, so the apparently “normal” spiral galaxies in the cluster center, which are photometrically more akin to field spirals than cluster spirals in nearby clusters (Andreon et al. 1997), could be going through bursts.

Of course it is of no surprise that starbursts are induced by some form of interaction; galaxy groups provide ideal environments for merger-induced star-forming activity. We now speculate if the occurrence of starbursts could be enhanced

specifically in cluster environments. X-ray observations show that Abell 851 is going through an on-going cluster-scale merger process, in which two X-ray emitting cores merging in about a few hundred Myr (Schindler & Wambsgans 1996; Schindler et al. 1998; De Filippis et al. 2003). Recent simulations have shown that galaxy clusters in  $\Lambda$ CDM cosmology have two distinct phases in mass accretion history, merger-dominated and accretion-dominated phases (Zhao et al. 2003). Major cluster mergers, involving almost doubling their total mass, is not rare at the redshift of Abell 851 (Tasitsiomi et al. 2004). Inferred star-forming property of cluster galaxies would show differences in each phase, adding possible complications to a pure infall scenario. The apparently complex spatial as well as velocity distributions of [O II] emitters in Abell 851 perhaps reflects such cluster-scale mixing of galaxy populations. Applying dynamical methods to such a dynamically active cluster poses difficulties as well; velocity dispersions are not a good indicator of cluster properties for dynamically active clusters going through mergers (Crone & Geller 1995).<sup>10</sup>

On the flip side of the complexity, there are some evidence that dynamically active clusters host a larger number of star-forming galaxies and AGNs (Lotz et al. 2003; Miller & Owen 2003; Rakos & Schombert 2005). As mentioned previously the existence of old galaxy population tracing clumpy distribution of substructures along filaments is generally confirmed in wide-field survey of Abell 851 using both photometric redshift method (K01) and cluster red-sequence technique (Kodama et al. 2005). The radial velocity distributions show weak, yet positive evidence for kinematic segregation between the cluster [O II] emitters and D99 k-type galaxies, when the samples are restricted within the core region (Fig. 3). Their spatial distributions, again restricted within the central region, clearly show an abundance of old galaxies where the cluster [O II] emitters only sparsely exist. Hence it is natural to interpret many [O II] emitters to be relatively new,

<sup>10</sup> As a result, the estimates for the virial radius of Abell 851 vary widely, and its unique dynamical center can not be rigorously determined. This is a major reason why we have stayed clear of analysis using cluster-centric radii.

recently accreted galaxies onto the cluster potential which already hosts many evolved galaxies. The non-Gaussian velocity distribution of cluster [O II] emitters also provides evidence that they represent a population that has not been virialized in the cluster potential. In general, it is unlikely that red, gas-poor galaxies such as cluster ellipticals get rekindled in starbursts, but a dominant contribution to cluster star-forming activity can easily come from gas-rich spiral galaxies infalling onto a cluster. Hence, the enhanced star-forming activity in the infall region, like that seen in the southern substructures in Fig. 18, probably is due to an increased frequency of galaxy-galaxy interactions between quiescent yet gas-rich galaxies, as the infalling groups themselves interact with nearby groups on the way to the cluster center. This is consistent with the high abundance of [O II] emitters *between* the apparent infalling groups in the southern filament.

Yet clusters offer means of interactions other than the ones between galaxies—the dense cluster gas in the core could ram-strip galaxies of their fuel supply, and the steep cluster gravitational potential could tidally interact with infalling galaxies. In CL0024+1652 at  $z \approx 0.4$ , Moran et al. (2005) found that morphologically early-type galaxies with large mass showed enhanced Balmer absorption lines within the cluster virial radius, while some fainter counterparts close to the virial radius actually showed [O II] emission. These authors rule out merger-induced star formation after inspection of their morphology (though they mention harassment is a potential triggering mechanism). In local Coma cluster, Poggianti et al. (2004) recently found an abundance of young post-starburst galaxies near the edges of X-ray substructures, indicating the interaction between cluster galaxies and intra-cluster medium could trigger star-forming activity. These observations imply the importance of interactions between infalling galaxies and environments specific to clusters. The X-ray observation by De Filippis et al. (2003) was probably not deep enough to trace the cluster gas much beyond the very center of Abell 851 (Fig. 19).

To summarize, in view of highly dynamically active state of Abell 851, the enhancement of star-forming activity seen in this cluster may be the result of accelerated gas consumption within infalling gas-rich galaxies driven by the galaxy-galaxy interactions in infalling group environments. As a favored triggering mechanism of starbursts, galaxy-galaxy harassment, as opposed to a major merger, appears consistent with preserving the disk morphology of cluster [O II] emitters, although the direct confirmation with our [O II]-emitting sample is limited only to the cluster central region due to the limited coverage of *HST* observations. For the rest with subtle or no morphological indication of interaction in the cluster central region, we can only speculate if an increased inhomogeneity in the distribution of intracluster gas/potential makes triggering star-forming activity more effective, such as in shocking the interstellar medium of galaxies.

### 6.3. Possible Role of AGNs as Firemen

Some optically-luminous [O II] emitters in the cluster central region shows a glimpse of the fate of cluster star-forming galaxies. To see how the [O II] emitters are distributed relative to the intracluster gas, in Fig. 19 we overlay X-ray emission contours, kindly provided by B. De Filippis. We see very few [O II] emitters in the region where the X-ray emission is very strong, although galaxies of the types associated with old stellar population are abundant (see Fig. 8). More remarkably, the [O II] emitters classified as AGN-like (in black squares)

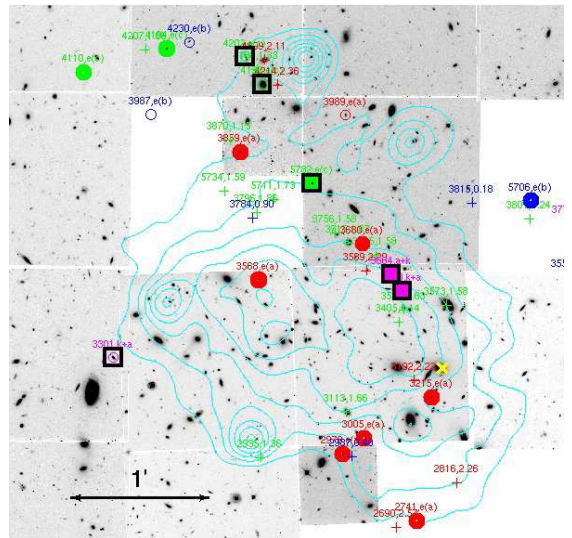


FIG. 19.— The distribution of cluster [O II] emitters in the central region of Abell 851 with the *HST* WFPC2 images. The north is up, and the east is in the left. The yellow cross denotes  $9^{\text{h}}42^{\text{m}}56^{\text{s}}.2$ ,  $46^{\circ}59'12''.0$  (J2000), from which  $\Delta\text{RA}$  and  $\Delta\text{DEC}$  are measured in Fig. 8. The overlaid contours in cyan are X-ray emission map from De Filippis et al. (2003). Those galaxies identified to be AGN-like are marked by black squares; otherwise the colors of the symbols denote D99 spectral classes as in Fig. 18. [See the electronic edition of the paper for a color version of this figure.]

appear to align themselves in a preferred direction from the south-west to the north-east. Whether this preferred axis has any physical significance is not obvious both from the figure and from the X-ray temperature map presented by De Filippis et al. (2003). Nonetheless we note that the cluster central field presented in Fig. 19 is a small fraction of the total survey area for our [O II] emission search but hosts six of the seven AGN-like galaxies in our sample; in comparison, only 20 out of 111 confirmed cluster [O II] emitters and 186 out of 808 K01 cluster members are in the region shown in Fig. 19.

We reiterate that our AGN identification is not very complete, i.e., the line-ratio diagnostics could be done only for a subset of all the cluster [O II] emitters. Furthermore, none of the AGN-like galaxies are spatially coincident with X-ray point sources identified by De Filippis et al. (2003); only one  $g-i > 2$  [O II] emission candidate (which was not followed up spectroscopically) from the MLF00 narrowband survey coincided with the point source #8 in De Filippis et al. The optical diagnostics are often inadequate for secure AGN identification; Martini et al. (2002), for example, have reported in Abell 2104 the optically-selected AGNs fraction is by a factor of 5 lower than that of the X-ray-selected—some X-ray-selected AGNs do not even show strong emission lines. On the other hand, a high X-ray column can give rise to X-ray-obscured, optically-identified AGNs (Brandt et al. 2004). Based on the fluxes of the X-ray point sources detected in their imaging, the *XMM* exposure time of 51 ks should have easily detected AGNs at the flux level of  $f_x (0.3-10.0 \text{ keV}) \gtrsim 10^{-14} \text{ erg s}^{-1} \text{ cm}^{-2}$ . To our knowledge it is not clear whether a reasonable level of high X-ray column can obscure AGNs to put our galaxies below this level of detection. Nonetheless the optical line ratio diagnostics does suggest a possibility that these AGN-like galaxies could harbor low-luminosity AGNs.

If these are in fact AGNs, a possible clue may be provided by a recent study by Yan et al. (2005), reporting that the [O II] emitters in red sequence and post-starburst galaxies in their low- $z$  SDSS sample seem to host AGNs/LINERs. In an independent study, Tremonti et al. (2006, private communica-



tion) similarly finds signs of AGN activity in their SDSS post-starburst galaxy sample. Spectral decomposition of an SDSS AGN sample by Vanden Berk et al. (2006) showed post-starburst activities to be much more common in broad-line AGNs. Interestingly, three of the AGN-like galaxies in our sample are classified into k+a/a+k, a post-starburst type, in the D99 spectral classification scheme, although the fact that they made into our [O II]-selected sample means they have residual [O II] emission. We also find most of the AGN-like galaxies in our sample reside in local environments whose galaxy densities are higher than the K01 threshold above which cluster galaxy colors are typical of red, non-star-forming population (although we must point out the K01 threshold characterizes the dense cluster central region, as well as infalling substructures where we find little evidence for AGN-like galaxies). Furthermore, their location on the color-magnitude diagram indicates they are among the most luminous [O II] emitters, but their  $g-i$  color is either indistinguishable from the rest of the [O II]-emitting population or consistent with being on the red sequence (Fig. 6). With the indications that the cluster red sequence building up from the luminous end in a downsizing fashion (De Lucia et al. 2004; Tanaka et al. 2005), there is a curious connection between AGNs as a mechanism for shutting off star formation and the property of host galaxies. Hence the distribution of AGN-like [O II] emitters in the color-magnitude diagram, along with their relatively smaller [O II] emission equivalent widths (Paper I), is consistent with the scenario in which the star-forming activities within luminous galaxies are shut off by AGNs. Similar observations of cluster star-forming galaxies over a wide range of redshifts could provide evidence for or against the role of AGNs in causing the downsizing trend, where quenching of star formation progressively move toward lower luminosity systems at lower redshifts.

Yet, it is a mystery as to why AGN-like galaxies are not seen in the [O II] emitters outside the cluster central region. The K01 threshold effect, if real, implies that galaxies can transform from star-forming to non-star-forming in group environments in infall regions. Six out of seven AGN-like galaxies in our sample are in high-density environments above the K01 threshold but are preferentially located in the cluster central region. Ruderman & Ebeling (2005) have generally found an excess of X-ray-selected AGNs in the core region in both relaxed and morphologically-disturbed clusters (plus another milder peak near virial radius in relaxed clusters). These observations might suggest the significance of the locations of galaxies within clusters, as well as the effect of local environments, in transforming the star-forming properties of cluster galaxies.

There also is an ambiguity as to whether their broadband  $i$  magnitudes are truly representative of the host galaxies. If AGNs are active, it is likely that they make a significant contribution to the continuum light in the optical, making host galaxies brighter than they really are. That the most AGN-like galaxies in our sample are among the brightest [O II] emitters might simply be a result of additional contributions to the continuum from AGN activities.

In view of the general difficulty in systematic AGN selection, the AGN-like galaxies in our [O II]-emitting sample do not offer direct evidence for the connection between quenching of star formation and AGN activity. Yet, the observed trends discussed here are all consistent with AGNs playing some role in the production of bright cluster ellipticals with little star-forming activity. In any case, a more robust AGN

identification and follow-up studies of these objects would be necessary to confirm this hypothesis.

#### 6.4. Interpretation of Faint [O II] Emitters

The analysis of composite spectra based upon sampling on the  $i$ - $\Sigma$  plane has shown relatively little variation with local galaxy density, except for the faintest [O II] emitters residing in the low-density environment, i.e., the LF subsample. The [O II] emitters in the other subsamples are mostly consistent with the e(a)-type and typically show higher  $H\delta$  absorption equivalent widths at  $\sim 4-5 \text{ \AA}$ , with relatively little scatter. The faint [O II] emitters in low-density environments show the [O II] and  $H\delta$  equivalent widths typical of e(b) spectrum indicating a very young, pure starburst.

$N$ -body simulations by Moore et al. (1999) demonstrated that the response of a spiral galaxy to the tidal disruption from the cluster potential and galaxy-galaxy interactions—galaxy harassment—varies depending on the concentration of the mass distribution and the disk scale length. Low surface brightness galaxies respond dramatically to the influence of both the local and global variations in the gravitational potential, while high surface brightness galaxies remain stable. We lack morphological information to see how  $i$  magnitude and mass concentration are related systematically in our sample, though faint  $g-i < 1$  [O II] emitters generally have small isophotal area, implying their dwarf identity (MLF00). The relative depletion of HF [O II] emitters in Fig. 5 could be evidence for destruction of star-forming dwarf galaxies in dense regions due to galaxy harassment. On the other hand, such an absence of faint star-forming population does not have to indicate the total absence of galaxies in the particular subset. The depletion of faint [O II] emitters in dense environments may just be a reflection of highly suppressed star-forming activity in dwarf galaxies. The dense intracluster medium can provide effective gas-removal mechanisms, such as ram-pressure stripping, which is also a very likely scenario for dwarfs with a more diffuse matter distribution. In this case galaxies are not destroyed but could simply fade out of  $i$  band flux limit as star formation ceases.

The contribution of dwarf galaxies to the total galaxy population has been studied in terms of galaxy luminosity functions (e.g., de Propris et al. 1998a; de Propris & Pritchet 1998b; Trentham & Tully 2002; Valotto et al. 2004; Popesso et al. 2005, 2006). Up to and below the magnitude limit relevant for the [O II] emitters studied in this paper, there are evidence for a steeper faint-end slope in nearby clusters than that of field luminosity functions, and a higher abundance of dwarf galaxies in clusters has been proposed as the cause of such steep cluster luminosity functions (e.g., de Propris et al. 1998a; de Propris & Pritchet 1998b). The detection of such a trend seems not universal, however, and there is even a suggestion that sample selection biases could cause a steeper faint-end slope (Valotto et al. 2004). Although it is still not clear how the general form of faint-end luminosity function differs systematically between clusters and field regions, *type-specific* luminosity functions appear to depend strongly on environment regardless of the precise form of luminosity function for the entire population: The brighter end is dominated by non-star-forming population, while the faint-end is very sensitive to the relative abundance of both star-forming and non-star-forming populations (Goto et al. 2002; De Propris et al. 2003).

Two major surveys, SDSS (Goto et al. 2002) and 2dFGRS (De Propris et al. 2003), disagree in their measurement of the

faint-end slope of the cluster luminosity function—flatter in SDSS and only slightly steeper in 2dFGRS. As far as the interpretation of where the star-forming dwarfs in high-density environments go, the behavior of the faint-end slope makes a profound difference. If the disappearance of star-forming faint dwarfs is simply due to their fading as in stripping of gas supply, an increase in the number of non-star-forming dwarfs would match the decrease in the star-forming population, and the shape of overall luminosity function would not change as much, consistent with 2dFGRS, finding non-star-forming population to increase and make the faint-end slope steeper (less complications arising from flux limits being sensitive to galaxies with different stellar populations). On the other hand, galaxy harassment can either destroy galaxies as in tidal debris (Moore et al. 1999) or *create* even smaller galaxies as in tidal dwarf galaxies (Popesso et al. 2006). Hence the behavior of the faint-end slope of luminosity function alone would still not distinguish these dwarf galaxy production models. Our sample is also insensitive to the surviving dwarf galaxies in the cluster central region, since they are likely to be stripped of their gas supply (Mori & Burkert 2000) and show no star formation.

Yet our data could offer insight as to at which point of cluster formation history the abundant cluster dwarf population is really produced. Since the metal enrichment ceases in such gas-poor dwarfs, comparing the gas-phase metallicities of dwarf galaxies in Abell 851 and local clusters may tell us if gas-rich dwarfs in  $z = 0.4$  clusters could be the progenitors of the abundant gas-poor dwarf galaxies in local clusters. We wish to present the metallicity analysis in our forthcoming paper of the series.

In short, our finding in Abell 851 merely shows high-density environments to be hostile to dwarf starburst galaxies. The reported increase in non-star-forming dwarfs in cluster central region (Thompson & Gregory 1993; De Propriis et al. 2003; Popesso et al. 2006) does not necessarily prefer one interpretation over another as to the fate of infalling star-forming dwarfs. The forth-coming metallicity analysis may provide some clues for addressing the progenitor-offspring issues surrounding cluster dwarf galaxies.

## 7. SUMMARY

We have reported on a spectroscopic follow-up study of narrowband-selected [O II] emitters in Abell 851 from the MLF00 catalog, focusing on their local environments, kinematics, and SFHs. Along with similar studies (e.g., Balogh et al. 2004a,b; Kodama et al. 2004; Rines et al. 2005), the cluster [O II] emitters reaffirm the fundamental importance of local environments: The fraction of galaxies with [O II] emission is a strong function of local galaxy density where few [O II] emitters are found in dense environments, yet the strength of [O II] equivalent width does not vary strongly with local galaxy density. The trends are consistent with the mechanisms that halt star-forming activity on short timescales or are sufficiently rare. In high-density environments, the cluster [O II] emitters appear to show distinct behaviors depending on their luminosity: For optically-luminous [O II] emitters in the cluster central region, there is some weak evidence for AGNs playing a role in suppressing star formation in the host galaxies. On the fainter end, we note the lack of faint [O II] emitters in dense environments; the destruction of dwarf galaxies in galaxy harassment (Moore et al. 1999) and/or simple fading of emission lines due to quenching of star formation in ram-stripped dwarfs (Mori & Burkert 2000) can cause such a

deficit. The luminosity-dependent behaviors of star-forming galaxies strongly suggest normal disk galaxies, which are predominantly e(a) galaxies, and dwarf galaxies, which are mostly pure bursting e(b) galaxies, respond quite differently within dense cluster environments.

The cluster [O II] emitters have shown the kinematic properties consistent with a non-virialized population; their velocity distribution deviates significantly from a Gaussian. The skewed distribution toward higher velocities is also consistent with a high fraction of the [O II] emitters being at first infall, as opposed to a backplash population which may have gone through the cluster central region in the past (e.g., Gill et al. 2005). We observe a greater fraction of cluster [O II] emitters with high radial velocities, compared to the emission-line galaxies in local clusters (Rines et al. 2005; Pimblet et al. 2006). In addition, their spatial distribution is highly asymmetrical with respect to the cluster center. These provide evidence for a significant fraction of the cluster [O II] emitters constituting an infalling population.

The spectral evolution modeling and the distribution of the cluster [O II] emitters in the [O II]-H $\delta$  plane highlight a dominant presence of dusty starburst galaxies [i.e., e(a)-type in the D99 scheme]. A high abundance of e(a) galaxies in clusters was already remarked by Poggianti et al. (1999), whose subsequent studies identified them as dusty starbursts, primarily caused by selective extinction of the light from very young stellar population (e.g., Poggianti & Wu 2000; Poggianti et al. 2001). A combination of stellar population synthesis and nebular photoionization codes favors models with star-forming timescales of order  $\lesssim 1$  Gyr for dusty galaxies,  $E(B-V) \gtrsim 0.5$ , for covering the distribution of cluster [O II] emitters in the [O II]-H $\delta$  equivalent width plane. The range of timescales, along with a higher occurrence of e(a) galaxies in Abell 851 compared to the field, is consistent with scenarios in which triggering of the starbursts is cluster-related. Existing morphological studies (Smail et al. 1997; Poggianti et al. 1999) further provide evidence for e(a) galaxies arising at the expense of regular star-forming galaxies [i.e., e(c)-type] by preserving their disk-like morphology. The redshift trend of the relative fractions of [O II] emitters in various D99 spectral classes also suggest a higher incidence of e(a) galaxies in Abell 851 compared to the field at a similar redshift.

The enhanced star-forming activities observed in Abell 851 may have some connections to the highly dynamically active state of the cluster. We specifically note a high abundance of [O II] emitters *between* two infalling groups located in the southern filament of Abell 851. The proximity of two groups during the process of an accretion onto the cluster may have caused the galaxies to interact at a higher frequency, although we lack high-resolution morphology to confirm signatures of interaction in these galaxies. An inhomogeneous intracluster gas distribution (De Filippis et al. 2003) might also increase the frequency of triggering of star-forming activity in the galaxies in the cluster central region; a direct confirmation of this additional hypothesis would need a larger inventory of morphology and spectra for the galaxies spatially coincident with a deep X-ray emission map. On the other hand, the archival *HST* morphology suggests galaxy-galaxy harassment is very effective in inducing a starburst even in the galaxies residing within the cluster central region. Galaxy harassment is also preferred over major mergers because of the assumed preservation of disk structures.



We are especially grateful to Tadayuki Kodama for sharing with us their photometric redshifts catalog of Abell 851, without which the detailed study of our sample in terms of local environments could not be carried out. We are also thankful to Betty De Filippis (for the X-ray contour map) and Francois Hammer and Hector Flores (for the CFRS spectra) for giving us an access to their data. We also thank the anonymous referee for numerous valuable comments which helped us make this a stronger paper. T.S. thanks Shane Davis, Colleen Schwartz, and Tommaso Treu for useful conversations on various topics which constituted portions of this paper. Financial support was provided by the David and Lucille Packard Foundation and the Alfred P. Sloan Foundation. This research has made use of the NASA/IPAC Extragalactic Database (NED), which is operated by the Jet Propulsion Laboratory, California Institute of Technology, under contract with the National Aeronautics and Space Administration. This research has made use of the NASA Astrophysics Data System abstract service. Funding for the DEEP2 survey has been provided by NSF grant AST-0071048 and AST-0071198. Funding for the Sloan Digital Sky Survey (SDSS) has been provided by

the Alfred P. Sloan Foundation, the Participating Institutions, the National Aeronautics and Space Administration, the National Science Foundation, the U.S. Department of Energy, the Japanese Monbukagakusho, and the Max Planck Society. The SDSS Web site is <http://www.sdss.org/>. The SDSS is managed by the Astrophysical Research Consortium (ARC) for the Participating Institutions. The Participating Institutions are The University of Chicago, Fermilab, the Institute for Advanced Study, the Japan Participation Group, The Johns Hopkins University, the Korean Scientist Group, Los Alamos National Laboratory, the Max-Planck-Institute for Astronomy (MPIA), the Max-Planck-Institute for Astrophysics (MPA), New Mexico State University, University of Pittsburgh, University of Portsmouth, Princeton University, the United States Naval Observatory, and the University of Washington. The authors wish to recognize and acknowledge the very significant cultural role and reverence that the summit of Mauna Kea has always had within the indigenous Hawaiian community. We are most fortunate to have the opportunity to conduct observations from this mountain.

*Facilities:* Keck:I (LRIS), Keck:II (DEIMOS)

## APPENDIX

### SPECTRAL EVOLUTION MODELING

We synthesized model galaxy spectra incorporating differential extinction of stellar continuum and nebular emission components. We used a combination of a stellar population synthesis code, GALAXEV version 2003 (Bruzual & Charlot 2003), and a nebular photoionization code, version 96.01a of Cloudy (Ferland et al. 1998). First, for each predefined SFH, GALAXEV was used to synthesize a series of spectra at various ages. Three SFHs are explored: instantaneous burst; constant burst of finite duration  $\tau$ , after which there is no star formation (i.e., truncation models); and exponentially-declining SFHs with various  $\tau$  (no gas recycling). The analytical forms of these SFHs are described in Bruzual & Charlot (2003). For the latter two SFHs, we used the values of  $\tau = 10, 10^2, 10^3$ , and  $2 \times 10^3$  Myr. We used the GALAXEV models with the Padova 1994 evolutionary tracks and assumed a Salpeter initial mass function ( $\mathcal{M} = 0.1\text{--}100M_{\odot}$ ) at solar abundance ( $X = 0.70, Y = 0.28$ , and  $Z = 0.02$ ). The standard GALAXEV output gives the production rates of hydrogen-ionizing photons,  $Q(\text{H})$ , which are scaled to the total mass of an ionizing source ( $\log \mathcal{M}_*/M_{\odot} \sim 2\text{--}9$ ). The mass of ionizing source therefore enters only as a scaling factor for  $Q(\text{H})$ . Thus constructed ionizing source spectrum energy distribution and properly scaled  $Q(\text{H})$  were fed to Cloudy for photoionization simulations.

In Cloudy, our model H II region is a single hydrogen-ionizing source surrounded by a spherical distribution of constant-density, ionization bounded nebula at the solar abundance. We used the solar abundance and depletion factors assumed by Kewley et al. (2001). The hydrogen density ( $n_{\text{H}} = 10 \text{ cm}^{-3}$ ), the volume filling factor ( $\epsilon = 1$ ), the covering factor ( $C = 1$ ), and the inner radius ( $r_{\text{in}} = 10^{-2}$  pc) to the nebula were all kept constant throughout the simulations with Cloudy. These parameters can be chosen rather arbitrary, since the ionization state of nebula is uniquely determined by the combination of the spectral energy distribution of ionizing source and the ionization parameter defined as

$$u = \frac{Q(\text{H})}{4\pi R_s^2 n_{\text{H}} c},$$

where  $R_s$  is the Strömgen radius and  $c$  is the speed of light, so long as the density remains below the limit for collisionally de-excitation cooling (see, e.g., Stasinska & Leitherer 1996).

Dust modeling features were generally turned off within these codes. We manually attenuated the stellar and nebular components by a different amount of extinction, adopting the attenuation curve of Calzetti et al. (2000, Eq. (8)). It has been shown empirically that the stellar continuum suffers roughly half of the extinction suffered by the nebular gas,  $E(B-V)_* \simeq 0.44E(B-V)_{\text{g}}$  (see Calzetti et al. 1994, and reference therein). This ratio was varied [ $E(B-V)_*/E(B-V)_{\text{g}} \equiv E_*/E_{\text{g}} = 0.22, 0.44$ , and  $0.88$ ] to see the effect of differential extinction on our measurements of equivalent widths. This is motivated by the interpretation of e(a) spectrum by Poggianti et al. (2001), requiring selective extinction of light from stellar populations of various ages. A range of extinction  $E(B-V) = 0.0\text{--}1.5$  was explored. Note that  $E(B-V) \equiv E(B-V)_{\text{g}}$  is the amount of extinction in the nebular component, being derived from a Balmer decrement (Paper I). Resulting synthesized spectra are used to measure [O II] and H $\delta$  equivalent widths using the flux-summing method (Paper I). The advantage of our method presented here is that both emission and absorption lines, each suffering a different amount of extinction, are modeled into the final spectra, which are measured with the same tool used for measuring other spectra.

We checked our method of simulation by running a simple model that closely resembles the solar abundance,  $M_T = 2 \times 10^4 M_{\odot}$  model published by Garcia-Vargas et al. (1995, Table 16), which has also been used by Moy et al. (2001) to check their simulation for consistency. Table A1 shows that the results generally agree well with each other.

Although our interest mainly lies in the evolution of spectral indices in the [O II]-H $\delta$  plane, we need some constraint on the relevant range of ionization parameter  $u$  so that our models roughly resemble the ionization state of nebulae in the observed

TABLE A1  
COMPARISON OF COUPLED-MODEL SIMULATIONS

Line	Models		
	This Paper <sup>a</sup>	M01 <sup>b</sup>	G95 <sup>c</sup>
$\log H\beta$ [erg s <sup>-1</sup> ]	38.79	38.83	38.84
[O II] $\lambda$ 3727/H $\beta$	3.12	3.10	3.07
[O II] $\lambda$ 5007/H $\beta$	0.32	0.31	0.25
[O I] $\lambda$ 6300/H $\beta$	0.07	0.04	0.04
[N II] $\lambda$ 6584/H $\beta$	1.29	1.34	1.34
[S II] $\lambda$ 6716/H $\beta$	0.70	0.57	0.58
[S II] $\lambda$ 6731/H $\beta$	0.49	0.39	0.40
[S III] $\lambda$ 9069/H $\beta$	0.31	0.36	0.34

NOTE. — The comparison of  $Z = Z_{\odot}$  instantaneous burst model at 1 Myr and  $\log u \simeq -3.11$ . The solar abundance is as defined in Garcia-Vargas et al. (1995).

<sup>a</sup>GALAXEV (version 2003) & Cloudy (version 96.01a).

<sup>b</sup>PEGASE.2 & Cloudy (version 90.04) by Moy et al. (2001).

<sup>c</sup>Cloudy (version unknown) and see Garcia-Vargas et al. (1995) for their stellar population synthesis models.

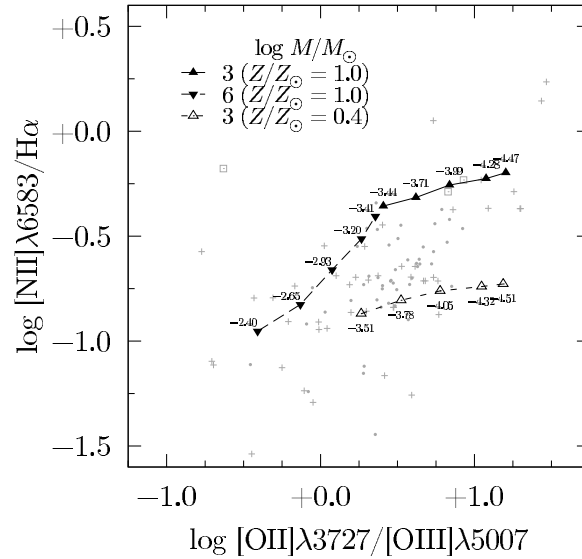


FIG. A1.— Emission line flux ratio  $[N II]\lambda 6583/H\alpha$  vs.  $[O II]\lambda 3727/[O III]\lambda 5007$  for three evolutionary model tracks. The numbers along each track indicate the ionization parameter  $u$  for each model. For each evolutionary track, data points appear at 1, 10,  $10^2$ ,  $10^3$ , and  $5 \times 10^3$  Myr from high to low  $u$ . Gray data points indicate the cluster [O II] emitters whose line ratios are computed from their highest-S/N spectrum (filled dots) and secondary spectrum (crosses). Squares indicate AGN-like galaxies. See Paper I for the definition of highest-S/N spectrum, secondary spectrum, and AGN-like galaxies; see Paper I.

In our models, the ionization parameter is essentially a function only of the production rate of hydrogen-ionizing photons  $Q(H)$ , and electron temperature  $T_e$ , namely

$$u = A(T_e) [Q(H)n_H\epsilon^2]^{1/3},$$

where  $A(T_e) \approx 2.8 \times 10^{-20} (10^4/T_e)^{2/3}$  (Stasinska & Leitherer 1996) and the  $T_e$  dependence comes from  $R_\nu$  (which depends on the recombination coefficient). Since the temperature varies within a nebula, we simply take the value of  $u$  computed by Cloudy at the end of each simulation. Hence adjusting  $u$  is done through one free parameter, the mass of central ionizing source with which  $Q(H)$  scales proportionally. Since the strength of [O II] $\lambda$ 3727 emission depends on the relative abundance of different oxygen ionic species, we constrained this by comparing the ratio  $[O III]\lambda 5007/[O II]\lambda 3727$  between the [O II] emitting sample and our simulated models. In Fig. A1 we see how solar-abundance models compare to observed galaxies. We first notice that any single model track between the ages  $t = (1-5) \times 10^3$  Myr does not span the range of observed [O II]/[O III] entirely, suggesting a need for variety of SFHs to explain the wide range of observed line ratios. Moreover, our models yield generally higher  $[N II]\lambda 6583/H\alpha$ . The ratio  $[N II]/H\alpha$  is sensitive both to the relative abundance of N to all other species and to the overall metal abundance of nebula, but it has relatively little effect on the observables in the [O II]-H $\delta$  plane. Although the line ratio diagram implies the cluster [O II] emitters may be at subsolar abundance in general, we chose solar-metallicity,  $M = 4M_{\odot}$  models at  $E(B-V) = 0.5$  and  $E_*/E_g = 0.44$  as our fiducial set of models.

#### REFERENCES

- Andreon, S., Davoust, E., & Heim, T. 1997, *A&A*, 323, 337
- Ball, N. M., Loveday, J., Brunner, R. J., Baldry, I. K., & Brinkmann, J. 2005, *ArXiv Astrophysics e-prints*, arXiv:astro-ph/0507547
- Balogh, M. L., Morris, S. L., Yee, H. K. C., Carlberg, R. G., & Ellingson, E. 1997, *ApJ*, 488, L75
- Balogh, M. L., Morris, S. L., Yee, H. K. C., Carlberg, R. G., & Ellingson, E. 1999, *ApJ*, 527, 54
- Balogh, M. L., Navarro, J. F., & Morris, S. L. 2000, *ApJ*, 540, 113
- Balogh, M. L., Baldry, I. K., Nichol, R., Miller, C., Bower, R., & Glazebrook, K. 2004a, *ApJ*, 615, L101
- Balogh, M., et al. 2004b, *MNRAS*, 348, 1355
- Balogh, M. L., Miller, C., Nichol, R., Zabludoff, A., & Goto, T. 2005, *MNRAS*, 360, 587
- Beers, T. C., Flynn, K., & Gebhardt, K. 1990, *AJ*, 100, 32
- Bekki, K. 1998, *ApJ*, 502, L133
- Blanton, M. R., et al. 2003, *AJ*, 125, 2348
- Bond, J. R., Kofman, L., & Pogossyan, D. 1996, *Nature*, 380, 603
- Brandt, W., Schneider, D., & Vignali, C. 2004, *ASP Conf. Ser.* 311: AGN Physics with the Sloan Digital Sky Survey, 311, 303
- Bruzual, G., & Charlot, S. 2003, *MNRAS*, 344, 1000
- Butcher, H., & Oemler, A. 1984, *ApJ*, 285, 426
- Calzetti, D., Kinney, A. L., & Storchi-Bergmann, T. 1994, *ApJ*, 429, 582
- Calzetti, D., Armus, L., Bohlin, R. C., Kinney, A. L., Koornneef, J., & Storchi-Bergmann, T. 2000, *ApJ*, 533, 682
- Cole, S., Aragon-Salamanca, A., Frenk, C. S., Navarro, J. F., & Zepf, S. E. 1994, *MNRAS*, 271, 781
- Colless, M., & Dunn, A. M. 1996, *ApJ*, 458, 435
- Couch, W. J., Ellis, R. S., Sharples, R. M., & Smail, I. 1994, *ApJ*, 430, 121
- Cowie, L. L., Songaila, A., Hu, E. M., & Cohen, J. G. 1996, *AJ*, 112, 839
- Crone, M. M., & Geller, M. J. 1995, *AJ*, 110, 21
- De Filippis, E., Schindler, S., & Castillo-Morales, A. 2003, *A&A*, 404, 63
- De Lucia, G., et al. 2004, *ApJ*, 610, L77
- de Propriis, R., Eisenhardt, P. R., Stanford, S. A., & Dickinson, M. 1998, *ApJ*, 503, L45
- de Propriis, R., & Pritchett, C. J. 1998, *AJ*, 116, 1118
- De Propriis, R., et al. 2003, *MNRAS*, 342, 725
- Diaferio, A., Kauffmann, G., Balogh, M. L., White, S. D. M., Schade, D., & Ellingson, E. 2001, *MNRAS*, 323, 999
- Dressler, A. 1980, *ApJ*, 236, 351
- Dressler, A., Oemler, A. J., Butcher, H. R., & Gunn, J. E. 1994, *ApJ*, 430, 107
- Dressler, A., Smail, I., Poggianti, B. M., Butcher, H., Couch, W. J., Ellis, R. S., & Oemler, A. J. 1999, *ApJS*, 122, 51 (D99)
- Dressler, A., Oemler, A. J., Poggianti, B. M., Smail, I., Trager, S., Shectman, S. A., Couch, W. J., & Ellis, R. S. 2004, *ApJ*, 617, 867
- Ebeling, H., Barrett, E., & Donovan, D. 2004, *ApJ*, 609, L49
- Ellingson, E., Lin, H., Yee, H. K. C., & Carlberg, R. G. 2001, *ApJ*, 547, 609
- Faber, S. M., et al. 2003, *Proc. SPIE*, 4841, 1657
- Ferland, G. J., Korista, K. T., Verner, D. A., Ferguson, J. W., Kingdon, J. B., & Verner, E. M. 1998, *PASP*, 110, 761
- Garcia-Vargas, M. L., Bressan, A., & Diaz, A. I. 1995, *A&AS*, 112, 35
- Gill, S. P. D., Knebe, A., & Gibson, B. K. 2005, *MNRAS*, 356, 1327
- Goto, T., et al. 2002, *PASJ*, 54, 515
- Gunn, J. E., Hoessel, J. G., & Oke, J. B. 1986, *ApJ*, 306, 30
- Hammer, F., et al. 1997, *ApJ*, 481, 49
- Icke, V. 1985, *A&A*, 144, 115
- Kauffmann, G., White, S. D. M., & Guiderdoni, B. 1993, *MNRAS*, 264, 201
- Kewley, L. J., Dopita, M. A., Sutherland, R. S., Heisler, C. A., & Trevena, J. 2001, *ApJ*, 556, 121
- Klypin, A., Kravtsov, A. V., Valenzuela, O., & Prada, F. 1999, *ApJ*, 522, 82
- Kodama, T., Smail, I., Nakata, F., Okamura, S., & Bower, R. G. 2001, *ApJ*, 562, L9 (K01)
- Kodama, T., Balogh, M. L., Smail, I., Bower, R. G., & Nakata, F. 2004, *MNRAS*, 354, 1103
- Kodama, T., et al. 2005, *PASJ*, 57, 309
- La Franca, F., et al. 2004, *AJ*, 127, 3075
- Le Fevre, O., Crampton, D., Lilly, S. J., Hammer, F., & Tresse, L. 1995, *ApJ*, 455, 60
- Le Flocc'h, E., et al. 2005, *ApJ*, 632, 169
- Lilly, S. J., Le Fevre, O., Crampton, D., Hammer, F., & Tresse, L. 1995, *ApJ*, 455, 50
- Lotz, J. M., Martin, C. L., & Ferguson, H. C. 2003, *ApJ*, 596, 143
- Mamon, G. A., Sanchis, T., Salvador-Solé, E., & Solanes, J. M. 2004, *A&A*, 414, 445
- Martin, C. L., Lotz, J., & Ferguson, H. C. 2000, *ApJ*, 543, 97 (MLF00)
- Martini, P., Kelson, D. D., Mulchaey, J. S., & Trager, S. C. 2002, *ApJ*, 576, L109
- Melnick, J., & Sargent, W. L. W. 1977, *ApJ*, 215, 401
- Mihos, J. C. 1995, *ApJ*, 438, L75
- Miller, N. A., & Owen, F. N. 2003, *AJ*, 125, 2427
- Moore, B., Lake, G., Quinn, T., & Stadel, J. 1999, *MNRAS*, 304, 465
- Moran, S. M., Ellis, R. S., Treu, T., Smail, I., Dressler, A., Coil, A. L., & Smith, G. P. 2005, *ApJ*, 634, 977
- Mori, M., & Burkert, A. 2000, *ApJ*, 538, 559
- Moy, E., Rocca-Volmerange, B., & Fioc, M. 2001, *A&A*, 365, 347
- Nakata, F., Bower, R. G., Balogh, M. L., & Wilman, D. J. 2005, *MNRAS*, 357, 679
- Oemler, A. J. 1974, *ApJ*, 194, 1
- Oke, J. B., et al. 1995, *PASP*, 107, 375
- Pimbblet, K. A., Drinkwater, M. J., & Hawkrigg, M. C. 2004, *MNRAS*, 354, L61
- Pimbblet, K. A., Smail, I., Edge, A. C., O'Hely, E., Couch, W. J., & Zabludoff, A. I. 2006, *MNRAS*, 366, 645
- Poggianti, B. M., Smail, I., Dressler, A., Couch, W. J., Barger, A. J., Butcher, H., Ellis, R. S., & Oemler, A. J. 1999, *ApJ*, 518, 576
- Poggianti, B. M., & Wu, H. 2000, *ApJ*, 529, 157
- Poggianti, B. M., Bressan, A., & Franceschini, A. 2001, *ApJ*, 550, 195
- Poggianti, B. M., Bridges, T. J., Komiyama, Y., Yagi, M., Carter, D., Mobasher, B., Okamura, S., & Kashikawa, N. 2004, *ApJ*, 601, 197
- Popesso, P., Biviano, A., Böhringer, H., & Romaniello, M. 2006, *A&A*, 445, 29
- Popesso, P., Böhringer, H., Romaniello, M., & Voges, W. 2005, *A&A*, 433, 415
- Rakos, K., & Schombert, J. 2005, *AJ*, 130, 1002
- Rines, K., Mahdavi, A., Geller, M. J., Diaferio, A., Mohr, J. J., & Wegner, G. 2001, *ApJ*, 555, 558
- Rines, K., Geller, M. J., Kurtz, M. J., & Diaferio, A. 2005, *AJ*, 130, 1482
- Ruderman, J. T., & Ebeling, H. 2005, *ApJ*, 623, L81
- Sanchis, T., Solanes, J. M., Salvador-Solé, E., Fouqué, P., & Manrique, A. 2002, *ApJ*, 580, 164
- Sato, T., & Martin, C. L. 2006, *ApJ*, accepted (Paper I)
- Schindler, S., & Wambsganss, J. 1996, *A&A*, 313, 113
- Schindler, S., Belloni, P., Ikebe, Y., Hattori, M., Wambsganss, J., & Tanaka, Y. 1998, *A&A*, 338, 843
- Shioya, Y., & Bekki, K. 2000, *ApJ*, 539, L29
- Smail, I., Dressler, A., Couch, W. J., Ellis, R. S., Oemler, A. J., Butcher, H., & Sharples, R. M. 1997, *ApJS*, 110, 213
- Solanes, J. M., Sanchis, T., Salvador-Solé, E., Giovanelli, R., & Haynes, M. P. 2002, *AJ*, 124, 2440
- Somerville, R. S. 2002, *ApJ*, 572, L23
- Stasinska, G., & Leitherer, C. 1996, *ApJS*, 107, 661
- Tanaka, M., Kodama, T., Arimoto, N., Okamura, S., Umetsu, K., Shimasaku, K., Tanaka, I., & Yamada, T. 2005, *MNRAS*, 362, 268
- Tasitsiomi, A., Kravtsov, A. V., Gottlöber, S., & Klypin, A. A. 2004, *ApJ*, 607, 125
- Thompson, L. A., & Gregory, S. A. 1993, *AJ*, 106, 2197
- Tran, K. H., Franx, M., Illingworth, G. D., van Dokkum, P., Kelson, D. D., & Magee, D. 2004, *ApJ*, 609, 683
- Tran, K.-V. H., Franx, M., Illingworth, G., Kelson, D. D., & van Dokkum, P. 2003, *ApJ*, 599, 865
- Trentham, N., & Tully, R. B. 2002, *MNRAS*, 335, 712
- Treu, T., Ellis, R. S., Kneib, J.-P., Dressler, A., Smail, I., Czoske, O., Oemler, A., & Natarajan, P. 2003, *ApJ*, 591, 53
- Valotto, C. A., Muriel, H., Moore, B., & Lambas, D. G. 2004, *ApJ*, 603, 67
- Vanden Berk, D. E., et al. 2006, *AJ*, 131, 84
- Willmer, C. N. A., et al. 2005, *ArXiv Astrophysics e-prints*, arXiv:astro-ph/0506041
- Yan, R., Newman, J. A., Faber, S. M., Konidaris, N., Koo, D., & Davis, M. 2005, *ArXiv Astrophysics e-prints*, arXiv:astro-ph/0512446
- Zhao, D. H., Mo, H. J., Jing, Y. P., Börner, G. 2003, *MNRAS*, 339, 12